Finite-size thermomechanical effects in smectic liquid crystals: The vapor pressure paradox as an anharmonic phenomenon

Lianghui Gao and Leonardo Golubović
Physics Department, West Virginia University, Morgantown, West Virginia 26506-6315, USA
(Received 10 May 2003; published 13 October 2003)

We pursue a systematic statistical mechanics study of finite smectic stacks of semiflexible manifolds bounded by interfaces under tension. We address, by analytic calculations and Monte Carlo simulations, the effects of the surface tension on smectic interlayer distances. We use our theoretical results to elucidate the so called vapor pressure paradox (VPP) in multilamellar membrane phases and explain the experiments of Katsaras [Biophys. J. **73**, 2924 (1997); **75**, 2157 (1998)]. We show that the effects of the interfacial tension are substantially weaker than suggested by the previous theoretical discussion of the VPP effects [R. Podgornik and V. A. Parsegian, Biophys. J. **72**, 942 (1997)]. By consistently taking into account the discrete, layered character of smectic liquid crystals, and anharmonic phonon effects, we show that the essence of VPP effects is in spatially nonuniform thermal expansion of smectic interlayer separations. We find that the average period of the whole finite stack can be both smaller (ordinary VPP effect at high enough interfacial tensions) or bigger (a reverse VPP effect at low interfacial tensions, overlooked in previous studies), relative to the average period of the corresponding infinite smectic stack. Looking at stacks from outside, these two effects show up as if there is an attractive (for the ordinary VPP effect), or repulsive (for the reverse VPP effect) pseudo-Casimir force acting between the two stack interfaces. We show however that the physics of VPP effects is obscured by schematically invoking Casimir-like forces. Rather, the ordinary and the reverse VPP effects are to be *both* characterized as *thermomechanical anharmonic effects caused by a spatially nonuniform thermal expansion of smectic interlayer distances*. Interlayer distances close to stack surfaces expand less (more) for the ordinary (reverse) VPP effect than those deep in the stack. The reverse VPP prevails at low interfacial tensions, simply because the membrane at the top of the stack is more free to fluctuate than membranes in the bulk. By increasing interfacial tension above a threshold value, fluctuations of the membrane at the stack top become suppressed, and the ordinary VPP effect prevails. In this study, we demonstrate that finite-size VPP effects in a strongly entropic system, such as the sterically stabilized lamellar phases, can be described quantitatively well by a simple analytic approach.

DOI: 10.1103/PhysRevE.68.041907 PACS number(s): 87.15.−v, 82.70.Uv, 82.70.Kj

I. INTRODUCTION

Smectic liquid crystals and smecticlike phases have been attracting attention of experimentalists and theorists for decades [1–13], in particular because of the biophysical significance of these systems [4–6,10,14–19]. Thermal fluctuations play a significant role in these systems. Typical examples for this are sterically stabilized smectic phases of large flexible manifolds, such as fluid membranes or semiflexible polymers interacting by purely hard-core repulsion [2,10–12,20–23]. In these phases, the restriction of the fluctuations of thermally rough manifolds by the presence of neighboring manifolds (hard-core interaction), yields the well known Helfrich effective (entropic) repulsion interaction [10]. In these so called unbound phases of manifolds, the smectic equation of state, which relates the isotropic osmotic pressure P to the smectic period a, is purely entropic in nature [11,12,22,23]. In particular, it predicts that the average smectic period a diverges for $P\rightarrow 0$. On the other side, thermal fluctuations are quantitatively significant also in the bound phases of manifolds, in which a remains finite for $P\rightarrow 0$, due to the presence of attractive intermanifold interactions [15–19]. In these bound phases, the actual (renormalized) value of the smectic phase period a may be substantially different from the mean-field estimate that minimizes the bare intermanifold potential. Here, the effect of thermal fluctuations is similar to the familiar thermal bond expansion in ordinary crystals. In smectic liquid crystals, however, such fluctuation effects are significantly stronger due to the soft character of these systems and thus a more prominent role is played by long-range thermal fluctuations.

Due to these reasons, the smectic ''bond length'' a may substantially depend also on the *size* of smectic systems, in particular, on the number of manifolds comprising the smectic stack, N. Thus, in two-dimensional (2D) sterically stabilized smectic phases of semiflexible polymers under isotropic osmotic pressure, the average stack period a_N is almost 10% *bigger* in small stacks ($N=2$ or 3) than in the bulk of an infinite stack ($N=\infty$), as revealed in our recent study Ref. [11]. In that study, the interfacial manifolds at the surfaces of the system are considered to be tensionless. Under some conditions, however, the smectic interfaces may acquire a nonzero surface tension γ. Classical examples for this are the multilamellar bilayer membrane phases that have interfaces corresponding to water-vapor-liquid interface (with the lamellar phase on the liquid side), or multilamellar phases with interfacial manifolds bound to solid substrates (corresponding to essentially infinite surface tension) [17,18]. For these systems, it has been pointed out by Podgornik and Parsegian [14] that the interfacial surface tension could suppress thermal fluctuations of the manifolds and thus substantially reduce the value of the average smectic period a_N of the N-manifold stack. This finite-size surface tension effect was argued to be quantitatively remarkably strong and vis-

ible even for macroscopically large values of N [14]. It was interpreted in terms of a long-range pseudo-Casimir attractive force between the system interfaces (as in Refs. [24,25]), and furthermore, it was suggested as an explanation for the so called *vapor pressure paradox* (VPP), frequently manifested in practice [14]: namely, in oriented smectic stacks with vapor-liquid or solid interfaces, it has been indeed noted that the smectic period a_N may be significantly smaller than the value a_∞ expected for the corresponding infinite systems, $N=\infty$. Such a period reduction may result from some other (not due to finite-size) effects, see Ref. [14]. Still, it has been argued that these other effects have been eliminated in the experiments with the systems exhibiting VPP phenomena. This has provided a basis to broadly adopt the theory of Podgornik and Parsegian [14] as an explanation of the VPP. However, a recent twist in this history of the VPP came from the careful experiments of Katsaras [17]. They have strikingly indicated that there is *no* VPP in multilamellar membrane phases in equilibrium with saturated water vapor. Thus, a new enigma emerged, on how to reconcile the existing theory of VPP with the recent experimental observations.

In this paper, we address this enigma by pursuing a systematic statistical mechanics study of finite stacks with N semiflexible manifolds bounded by interfaces under tension. We address, by analytical calculations and numerical simulations, the finite-size effects of the surface tension on the smectic period, i.e., the average interlayer distance. We find that these effects are substantially weaker than suggested by the previous theoretical discussion of the VPP phenomena in Ref. [14]. Within our theory of VPP in finite smectic liquid crystals, these systems are described more microscopically, as stacks of interacting manifolds, [11,12,20,22,23,26]. This is in contrast to the standard Landau-Peierls smectic continuum elastic model that has been employed in Ref. [14]. This classical continuum (elastic) model essentially ignores the discrete, *layered* character of smectic liquid crystals. Its formal application in Ref. [14] yields a strong dependence of the strength of the VPP on the microscopic short-distance cutoff of the manifolds Δx (such as the lipid molecule size). In fact, the presence of the experimentally small Δx in the quantitative results of Podgornik and Parsegian [14] is the main source for their remarkably large estimates of the strength of the VPP effect in equilibrium smectic liquid crystals: Within their theory, the strength of the VPP effect was actually found to diverge in the continuum limit $\Delta x \to 0$ [14]. Moreover, the application of the theory of Podgornik and Parsegian to the unbound, sterically repelling smectic stacks of membranes yields a strange conclusion that the intermembrane separation (smectic period) a_N reaches a finite value $(a_N)_{max} \sim \Delta x \sqrt{N}$ in the limit of zero osmotic pressure, $P \to 0$ [14]. Here, we find that these features are artifacts of formally using the smectic continuum model in Ref. [14]. In fact, the *more* microscopic smectic stack model, used by us here (and also in Refs. [11] and [12]), has *finite* continuum limit $\Delta x \to 0$, and thus only a weak dependence of the smectic period on the microscopic manifold cutoff Δx. In the result, the magnitude of the VPP effect we find is small, making it hardly observable in the stacks with $N \approx$ few hundred manifolds, in accord with the aforementioned experiments of Katsaras (see Secs. II and III). Importantly, this conclusion holds even for the *infinite* surface tension γ, or, equivalently, for the smectic liquid crystals fluctuating over solid surfaces (substrates). In fact, by using our smectic stack model, we find that the VPP effect has well defined, finite limit for $\gamma \to \infty$, see Secs. II and III. Here, we elucidate this important limit which may be nearly reached in realistic smectic systems with vapor-liquid interfaces. Recently, Nagle and Katsaras [18] put forward a qualitative picture of VPP effects, aimed to reconcile the difference between the experiments [17] and the theory of Ref. [14]. This picture suggests a mechanism weakening the VPP effect, by invoking the unbinding of the vapor-liquid interface from the stack. We find however that the VPP effect is *anyway* quantitatively weak in the stacks with $N=100$ or more manifolds, *even* if the high surface tension vapor-liquid interfaces are strongly bound to the stack. Another interesting prediction of our study is the existence of a *reverse* VPP effect that occurs in a range of *small* surface tensions γ (see Secs. II and III), or for vapor-pressure interfaces weakly coupled to smectic stacks (see Sec. IV). Under these conditions, we find that the average smectic period a_N of finite smectic stacks ($N<\infty$) is actually *bigger* than the average period of infinite smectic systems, a_∞. We find that the ordinary VPP phenomenon, with a_N *smaller* than a_∞, requires interfacial tensions γ exceeding a critical threshold value γ^* (in the model of Secs. II and III), or a strong enough coupling between the smectic stack and vapor-liquid interface (see Sec. IV). The threshold surface tension $\gamma^* = O(1)\delta\gamma$, where $\delta\gamma$ is the well known ''elastic'' surface tension of the interface of semi-infinite smectic liquid crystals [12,13], see Sec. II. *Only* for $\gamma \approx \gamma^* \approx \delta\gamma$, finite smectic stacks ($N<\infty$) are nearly uniform, with $a_N \approx a_\infty$ (see the end of Sec. II and our recent study [12]). Otherwise, for γ smaller (bigger) than γ^*, a_N is bigger (smaller) than a_∞, and the reverse (ordinary) VPP effect prevails.

An important feature of the study presented here is the calculation of the spatially *nonuniform* smectic layer spacings. We calculate them here as the function of the distance from smectic surfaces. Such a calculation has not been done in the previous studies of the VPP phenomenon. Thus, the theory of Podgornik and Parsegian [14] effectively assumes that the smectic spacings are uniform throughout the whole system. We show here that this is a grossly oversimplified picture, see Secs. II and III. In fact, we find that VPP phenomena themselves, i.e., the dependence of the smectic average period on the system size N, is, in large part, related to the behavior of nonuniform smectic spacings in the regions close to the smectic surfaces as discussed in Secs. II and III. This feature imposes severe limitations on the experimental observations of the VPP phenomena (see Sec. IV).

In this study, we show that invoking schematic similarities to standard pseudo-Casimir effects, as done in Ref. [14], obscures the real nature of the VPP effects, such as the important role played by (i) the layered character and (ii) the anharmonic effects in smectic liquid crystals. By consistently taking into account these two features, we show that VPP effects are *thermomechanical anharmonic finite-size effects* caused by *spatially nonuniform thermal expansion of smectic*

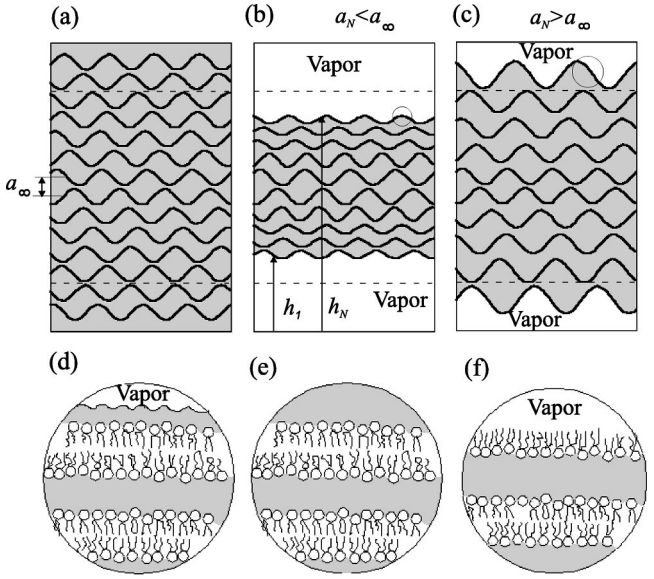

FIG. 1. (a) Manifold configurations close to the center of an infinite ($N=\infty$) smectic stack, with the average period a_∞. (b) and (c) depict a finite stack of N fluctuating manifolds (here $N=10$), with the average period $a_N=\langle h_N-h_1\rangle/(N-1)$. (b) depicts the ordinary VPP effect, with $a_N<a_\infty$, that occurs at large enough interfacial tensions. (c) depicts the reverse VPP effect, with $a_N>a_\infty$, that occurs at small enough interfacial tensions. (d) through (f) magnify three different situations at the stack interface. (d) There is a water layer between the outmost manifold and vapor, i.e., the water-vapor interface is bound to the outmost manifold (lipid bilayer). (e) There is no vapor, i.e., the water-vapor interface is unbound from the outmost lipid bilayer. (f) The outmost manifold is a lipid monolayer with tails in the vapor.

interlayer distances, as detailed in Sec. II. Here, we go beyond the previous schematic physical picture of VPP phenomena that has attempted to formally reduce them to pseudo-Casimir effects [14]. Essential for the physical understanding of VPP effects are the spatially nonuniform smectic interlayer distances which vary in magnitude as one moves from the stack surface to the center of the stack, as depicted in Fig. 1 (see Secs. II and III). In particular, the aforementioned reverse VPP effect is an anharmonic effect easily understood by considering the case of a membrane stack with zero surface tension at the stack interfaces. In this case all membranes are tensionless, and the major difference between membranes is in their coordination number, i.e., the number of their neighboring membranes. It is 1 for the two membranes at the bottom and the top of the stack, and it is 2 for other membranes. Because of this basic yet very important difference in the membrane confinement, the interlayer separation of the membrane at the stack surface (with just one neighbor) fluctuates more strongly than those of other membranes in the bulk (that are confined by two neighbors and thus have more constrained fluctuations). Due to this, thermal expansion (an anharmonic effect) of the interlayer distances is bigger close to stack surfaces than in the stack center (in the bulk), where the interlayer distance is close to its thermodynamic limit a_∞ [see Figs. 1(a) and 1(c)]. Hence, for zero or small enough surface tensions, the average period of the whole finite stack, a_N, is bigger than the bulk (thermodynamic limit) stack period of the corresponding infinite stack, a_∞, and one has the reverse VPP effect in Fig. 1(c). By looking at the finite stack *from the outside*, this finite-size anharmonic effect looks like an effect of a repulsive Casimir force acting between stack surfaces. However, the physical origin of our reverse VPP effect is in the nonuniformity of interlayer distances arising because the surface membrane is more free to fluctuate than other membranes [see Fig. 1(c)]. Moreover, even the ordinary VPP effect, interpreted as the ''mechanical Casimir effect'' by Podgornik and Parsegian, is *also* more deeply related to the nonuniformity of interlayer distances. This point is obscured in the theory of Podgornik and Parsegian [14], by assuming that the smectic interlayer distances are uniform throughout the system. Only from the anharmonic theory presented in the present study, it becomes clear that the ordinary VPP effect is also intimately related to the nonuniformity of smectic interlayer distances [see Fig. 1(b)]: Here, large enough surface tension suppresses fluctuations of the membrane at the top of the stack. Consequently, thermal expansion of interlayer distances is smaller close to the stack surfaces than in the bulk. Thus, for large enough interfacial tensions, the average period of the whole finite stack, a_N, is smaller than the bulk (thermodynamic limit) period of the corresponding infinite stack, a_∞ [see Figs. 1(a) and 1(b)]. From the outside, this ordinary VPP effect in Fig. 1(b) appears as a stack contraction due to some attractive pseudo-Casimir force between stack surfaces. But, from the outside, one cannot see the spatially nonuniform smectic interlayer distances underlying the VPP effect. Thus, reducing VPP effects to mechanical Casimir effects, as suggested by Podgornik and Parsegian [14], obscures the real physical character of these effects. We elucidate these findings by our analytic theory (Sec. II), and document our results rigorously by Monte Carlo simulations of the stacks of semiflexible manifolds (Sec. III). The simulations clearly show the presence of the reverse VPP effect for small surface tensions (in accord with the analytical theory of Sec. II). At large enough surface tension, our simulations document the ordinary VPP effect with a magnitude in accord with the analytic theory of Sec. II. We note that the reverse VPP effect has been noticed already before, in our recent study [11], for the special case of zero surface tension. It may be unsurprising to see such an anharmonic effect that emerges simply because the membrane at the top of the stack is more free to fluctuate, and thus acquires a larger intermembrane spacing (i.e., larger thermal bond expansion) than the membranes deep in the stack [see Fig. 1(c)]. This effect is washed out by modeling the stack as a formal harmonic continuum (employed in the theory of Podgornik and Parsegian [14]). By ignoring the layered character of the stack, effects such as our reverse VPP are simply lost due to formal continuum approach to the problem. Likewise, ignoring the realistic, layered character of smectic liquid crystals directly causes the huge overestimate of the strength of the ordinary VPP effect and aforementioned artifacts of the theory of Podgornik and Parsegian, such as the finite swelling of sterically stabilized lamellar phases of purely repelling membranes. These problems of the old theory of VPP effects, as well as the experi-

ments of Katsaras [17], have urged the development of the consistent theory of VPP phenomena presented in this paper.

The organization of this paper is as follows. In Sec. II, we introduce the smectic stack model and derive our analytic predictions for the VPP effects. In Sec. III, we address these effects by an exact scaling analysis and by Monte Carlo simulations of entropically dominated smectic systems such as the sterically stabilized lamellar phases. In that section, we show that finite-size effects in these strongly entropic systems can be described quantitatively well by means of a simple analytic theory. In Sec. IV, we further discuss and summarize our findings. Some important details of our calculations are discussed in Appendixes A and B.

II. FINITE SMECTIC STACKS: ANALYTIC PREDICTIONS FOR NONUNIFORM INTERLAYER SPACINGS

In this section, we discuss finite $(d+1)$-dimensional smectic stacks of N fluctuating d-dimensional semiflexible manifolds under an external isotropic osmotic pressure P, see Fig. 1. The microscopic smectic Hamiltonian for this stack of interacting manifolds is

$$H = H_{bulk} + H_{surf}. \tag{2.1}$$

Here, the first term, the smectic bulk Hamiltonian has the usual form [11]

$$\begin{aligned} H_{bulk}(\{h_n\}) &= \int d^d\mathbf{x} \Bigg\{ \sum_{n=1}^{N-1} [P\cdot(h_{n+1}(\mathbf{x}) - h_n(\mathbf{x})) \\ &\quad + V(h_{n+1}(\mathbf{x}) - h_n(\mathbf{x}))] \\ &\quad + \sum_{n=2}^{N-1} \frac{\kappa}{2} \left(\frac{\partial^2 h_n(\mathbf{x})}{\partial \mathbf{x}^2} \right)^2 \Bigg\}, \end{aligned} \tag{2.2}$$

with $h_n(\mathbf{x})$ describing the nth manifold height function above d-dimensional $\mathbf{x}$ plane (base plane). In Eq. (2.2), V is an intermanifold interaction potential. Note that, by Eq. (2.2), the external osmotic pressure P contributes the free energy term $P\times$(stack volume) [11]. Physically significant realizations of this model are 3D multilamellar phases of membranes $(d=2)$, and 2D smectic phases of semiflexible polymers $(d=1)$. κ in Eq. (2.2) is the manifold bending rigidity. The thermodynamic properties of this smectic stack model have been discussed in detail in Ref. [11], for the case of tensionless interfacial manifolds. The second term in Eq. (2.1), the stack surface contribution is given by

$$\begin{aligned} H_{surf}(h_1, h_N) = \int \frac{d^d q}{(2\pi)^d} [K^{(1)}_{surf}(q) |\tilde{h}_1(\mathbf{q})|^2 \\ + K^{(N)}_{surf}(q) |\tilde{h}_N(\mathbf{q})|^2], \end{aligned} \tag{2.3}$$

where $K^{(1)}_{surf}(q)$ and $K^{(N)}_{surf}(q)$ are the surface dispersion relations of the stack interfacial manifolds h_1 and h_N [$\tilde{h}_n(\mathbf{q})$ is the Fourier transform of $h_n(\mathbf{x})$]. The form of these dispersion relations depends on the nature of the system interfaces, as illustrated in Fig. 1, for the case of 3D multilamellar phases of lipid bilayer membranes $(d=2)$. If there is a thin water layer between the outmost manifold and vapor, and the water-vapor interface is *strongly* bound to outmost manifold (for whatever reason) as in Fig. 1(d), the appropriate form of K_{surf} is

$$K^{(N)}_{surf}(q) = \kappa q^4 + \gamma q^2 \tag{2.4}$$

with γ being the surface tension between water and vapor. As noted by Nagle and Katsaras [18], under some conditions, the vapor-water interface may unbind from the outmost manifold and move away from it, as depicted in Fig. 1(e). For this case, the surface dispersion relation is simply that of the bilayer, $K^{(N)}_{surf}(q) = \kappa q^4$, i.e., the surface manifolds are (also) tensionless. Finally, the surface manifold may be a monolayer membrane with hydrophobic lipid tails in the vapor, see Fig. 1(f). For this case, $K^{(N)}_{surf}(q) = \kappa_{mono} q^4 + \gamma q^2$ with $\kappa_{mono} \approx \kappa/2$, and γ is typically significantly smaller than the water-vapor surface tension. In Sec. IV, we detail on these complex phenomena and their influence on finite size-effects in smectic liquid crystals. In this section, we will focus on the basic model with the simple interface dispersion relation given by Eq. (2.4). For concreteness, here we consider the symmetric stacks as in Fig. 1, with $K^{(1)}_{surf}(q) = K^{(N)}_{surf}(q)$. An essential feature of our discussions here is consistent incorporation of the smectic discreteness, i.e., of the layered character of smectic liquid crystals. This is done by describing smectic liquid crystals microscopically, as stacks of interacting manifolds rather than by using the continuum Landau-Peierls model employed in Ref. [14] to discuss the VPP effects. Within harmonic phonon theory, such stacks have been discussed by Holyst and other authors [26]. Already at harmonic level, the incorporation of smectic discreteness may bring new insights into smectic physics, as exemplified by the study of Lei *et al.*, [27]. Anharmonic effects in stacks have been also studied, in particular, in the investigations of sterically stabilized phases of semiflexible polymers and fluid membranes [11,12,20,22,23], and in the studies of closely related strongly entropic membrane systems [15,16], such as the recent work of Manciu and Ruckenstein [15] discussing the equation of state of a small stack with two bilayer membranes. In the discussions that follow hereafter, by consistently taking into account the discrete, layered character of smectic liquid crystals and anharmonic phonon effects, we will show that the essence of the VPP effects (see the Introduction) is in spatially nonuniform thermal expansion of smectic interlayer distances, which vary in magnitude as one moves from the stack interfaces towards the stack center. In other words, VPP effects are elucidated here as thermomechanical anharmonic finite-size effects present in finite smectic stacks of N semiflexible manifolds (such as membranes or semiflexible polymers). By considering these anharmonic effects, we will find here that the average period of the whole finite stack can be both smaller (*ordinary VPP effect* at high enough interface tensions) or bigger (*reverse VPP effect* at low interface tensions), relative to the average period of the corresponding infinite $(N=\infty)$ smectic stack.

The presence of the surface tension γ may have substantial finite-size effects on various quantities of smectic systems, such as the average interlayer distances

$$a_N(n)=\langle h_{n+1}(\mathbf{x})-h_n(\mathbf{x})\rangle_{P,N,\gamma}, \tag{2.5}$$

and the average smectic period of the whole finite stack,

$$a_N=\frac{1}{N-1}\sum_{n=1}^{N-1} a_N(n)=\left\langle \frac{h_N(\mathbf{x})-h_1(\mathbf{x})}{N-1}\right\rangle_{P,N,\gamma}, \tag{2.6}$$

i.e., the equation of state relating a_N and P for any given N. Indeed, the surface tension tends to suppress fluctuations of manifolds close to stack surfaces. With increasing γ we thus expect to encounter a crossover between our reverse VPP effect ($a_N>a_\infty$, at low γ) and the ordinary VPP effect ($a_N<a_\infty$, at high γ), which has been anticipated in the Introduction (see Fig. 1). To study the behavior of $a_N(\gamma)$ as the function of N and γ analytically, in this section we will assume that the net intermanifold potential $V_{net}(r)=V(r)+Pr$ in Eq. (2.2) [$r=h_{n+1}(\mathbf{x})-h_n(\mathbf{x})$] has analytic minimum at r_0 and expand it in powers of $r-r_0$,

$$V_{net}(r)=V(r)+Pr=\sum_{k=0}^{\infty}\frac{b_k}{k!}(r-r_0)^k,$$

with $b_k=d^kV_{net}(r_0)/dr_0^k$ ($b_1=0$). By truncating this expansion to the quadratic order, one obtains the standard harmonic approximation to the smectic Hamiltonian [26]. Within the harmonic approximation [26] , the average interlayer distances, Eq. (2.5) are independent of N and n, and all equal to r_0. Nonuniformity of smectic interlayer distances, i.e., the dependence of $a_N(n)$ on N and n, may emerge due to the anharmonic terms in the expansion of V_{net}, such as the cubic term $b_3(r-r_0)^3/3!$ and higher-order terms [11]. $a_N(n)$ can be calculated systematically via the loop expansion in powers of the temperature T, see Appendix A (also, Ref. [11], Appendix). To the lowest [$O(T^1)$], one-loop order, one thus obtains

$$a_N(n,\gamma)=r_0-\frac{b_3}{2b_2}\langle[u_{n+1}(\mathbf{x})-u_n(\mathbf{x})]^2\rangle_0, \tag{2.7}$$

for average interlayer distances Eq. (2.5), and

$$a_N(\gamma)=r_0-\frac{b_3}{2b_2}\frac{1}{N-1}\sum_{n=1}^{N-1}\langle[u_{n+1}(\mathbf{x})-u_n(\mathbf{x})]^2\rangle_0, \tag{2.8}$$

for the average smectic period of the whole stack, Eq. (2.6). In Eqs. (2.7) and (2.8), u_n is the manifold displacement from the $T=0$ equilibrium position [$h_n(\mathbf{x})=nr_0+u_n(\mathbf{x})$]. The equilibrium average in Eq. (2.7) is done with respect to the harmonic smectic elastic Hamiltonian

$$H_0=\int d^d\mathbf{x}\left[\sum_{n=1}^{N}\frac{\kappa}{2}\left(\frac{\partial^2u_n(\mathbf{x})}{\partial\mathbf{x}^2}\right)^2+\sum_{n=1}^{N-1}\frac{b_2}{2}[u_{n+1}(\mathbf{x})-u_n(\mathbf{x})]^2+\frac{\gamma}{2}\left(\frac{\partial u_1}{\partial\mathbf{x}}\right)^2+\frac{\gamma}{2}\left(\frac{\partial u_N}{\partial\mathbf{x}}\right)^2\right]. \tag{2.9}$$

For derivation and a simple physical interpretation of Eq. (2.7), see Appendix A.

The second term in Eqs. (2.7) and (2.8), with typically $b_3<0$, is just the thermal "bond expansion" of the local smectic layer spacing $a_N(n,\gamma)$ away from its $T=0$ value r_0. Importantly, this bond expansion is *nonuniform*, i.e., $a_N(n,\gamma)$ is n dependent, as depicted in Fig. 1. Indeed, as detailed in Appendix A, the intermanifold distance $a_N(n,\gamma)$ and average smectic period $a_N(\gamma)$ are found [by Eqs. (2.7) and (2.8)] to be of the form

$$a_N(n,\gamma)=a_\infty+A_d'[I_N(n,d,\bar{\gamma})-I_\infty(d)] \tag{2.10}$$

and

$$a_N(\gamma)=a_\infty+A_d'[I_N(d,\bar{\gamma})-I_\infty(d)]. \tag{2.11}$$

Here

$$a_\infty=r_0+A_d'\ I_\infty(d) \tag{2.12}$$

is the average smectic bulk ($N=\infty$) period. In Eqs. (2.10) and (2.11), $\bar{\gamma}$ signifies a dimensionless surface tension, defined via

$$\bar{\gamma}=\frac{\gamma}{\delta\gamma}. \tag{2.13}$$

Here,

$$\delta\gamma=\sqrt{\kappa b_2} \tag{2.14}$$

is the characteristic smectic surface tension scale, see Refs. [9,12,13], and our discussions at the very end of this section. For a finite N, the smectic interlayer spacings are different from its bulk value a_∞ in Eq. (2.12), as indicated by Eqs. (2.10) and (2.11), with

$$I_N(n,d,\bar{\gamma})=\int_0^1 dR\,\frac{(1-R)^{d/2-1}}{R^{d/4}}\,\frac{\left(1-\dfrac{[Z(R,\bar{\gamma})]^2}{R^3}R^{2(N-2)}\right)+\dfrac{1}{2}\dfrac{Z(R,\bar{\gamma})}{R^2}(R-1)(R^{2(n-1)}+R^{2(N-1-n)})}{1-\dfrac{[Z(R,\bar{\gamma})]^2}{R^2}R^{2(N-2)}}, \tag{2.15}$$

and

$$I_N(d,\bar{\gamma})=\frac{1}{N-1}\sum_{n=1}^{N-1} I_N(n,d,\bar{\gamma})=\int_0^1 dR\,\frac{(1-R)^{d/2-1}}{R^{d/4}}\,\frac{\left(1-\dfrac{[Z(R,\bar{\gamma})]^2}{R^3}R^{2(N-2)}\right)-\dfrac{1}{N-1}\dfrac{Z(R,\bar{\gamma})}{R^2}\dfrac{1}{1+R}(1-R^{2(N-1)})}{1-\dfrac{[Z(R,\bar{\gamma})]^2}{R^2}R^{2(N-2)}}, \tag{2.16}$$

with

$$Z(R,\bar{\gamma})=R^2\frac{\bar{\gamma}\sqrt{R}-R}{\bar{\gamma}\sqrt{R}+1}, \tag{2.17}$$

see Appendix A. In Eqs. (2.10)–(2.12), the quantities

$$A_d'=-\frac{b_3}{2b_2}\frac{S_d}{(2\pi)^d}\frac{k_BT}{2b_2}\left(\frac{b_2}{\kappa}\right)^{d/4} \tag{2.18}$$

[with S_d being the area of the d-dimensional unit sphere], $I_\infty(d)=B(1-d/4,d/2)$, and a_∞ are all independent of the surface tension γ. A_d' in Eq. (2.18) is typically positive, i.e., $b_3<0$, i.e., smectic bulk period Eq. (2.12) typically expands due to thermal fluctuations, $a_\infty>r_0$ (see Ref. [11] and the discussions in the following). We stress that the only γ-dependent terms in Eqs. (2.10) and (2.11) are the integrals $I_N(n,d,\bar{\gamma})$ and $I_N(d,\bar{\gamma})$. Their presence induces a dependence of the average interlayer distance $a_N(n)$ on the surface tension γ. Far away from the system's surface ($N\gg n\gg 1$), the dependence of $a_N(n)$ on γ and n disappears in the thermodynamic limit $N\to\infty$. Indeed, by Eqs. (2.10)–(2.14), one can easily show that

$$\lim_{n\to\infty}\lim_{N\to\infty} I_N(n,d,\bar{\gamma})=I_\infty(d),$$

and thus

$$\lim_{n\to\infty}\lim_{N\to\infty} a_N(n,d,\gamma)=a_\infty.$$

Likewise, for $N\to\infty$, the average smectic period a_N in Eq. (2.11) approaches its bulk value a_∞. This is illustrated in Fig. 2 which gives the ratio of $I_N(d,\bar{\gamma})/I_\infty(d)$ for $d=1$ and $d=2$, for various values of the dimensionless surface tension $\bar{\gamma}$ [obtained by numerically integrating Eq. (2.16)]. Apparently from this figure, this ratio approaches 1 for whatever values of $\bar{\gamma}$, and thus, by Eq. (2.11), $a_N\to a_\infty$ in the thermodynamic limit $N\to\infty$. From Fig. 2 and Eq. (2.11), the stack average period $a_N(\gamma)$ has an interesting dependence on the surface tension γ: Note that $I_N(d,\bar{\gamma})>I_\infty(d)$ in a range of small values of $\bar{\gamma}$, and $a_N(\gamma)$ is thus *bigger* than its bulk value a_∞. On the other side, from Fig. 2, to have $a_N(\gamma)<a_\infty$, the dimensionless tension $\bar{\gamma}$ needs to be bigger than a critical threshold value $\bar{\gamma}^*=O(1)$, as detailed in the following [see Eqs. (2.29)–(2.34)]. Furthermore, the average interlayer spacings $a_N(n)=\langle h_{n+1}(\mathbf{x})-h_n(\mathbf{x})\rangle$ in Eq. (2.10) also have an interesting dependence on the dimensionless surface tension $\bar{\gamma}=\gamma/\delta\gamma$. This is illustrated in Fig. 3, giving the numerically obtained ratio $I_N(n,d,\bar{\gamma})/I_\infty(d)$ for the $N=20$ manifolds stack. From Eq. (2.10), the local interlayer spacings $a_N(n)$ essentially follow this ratio as a function of n.

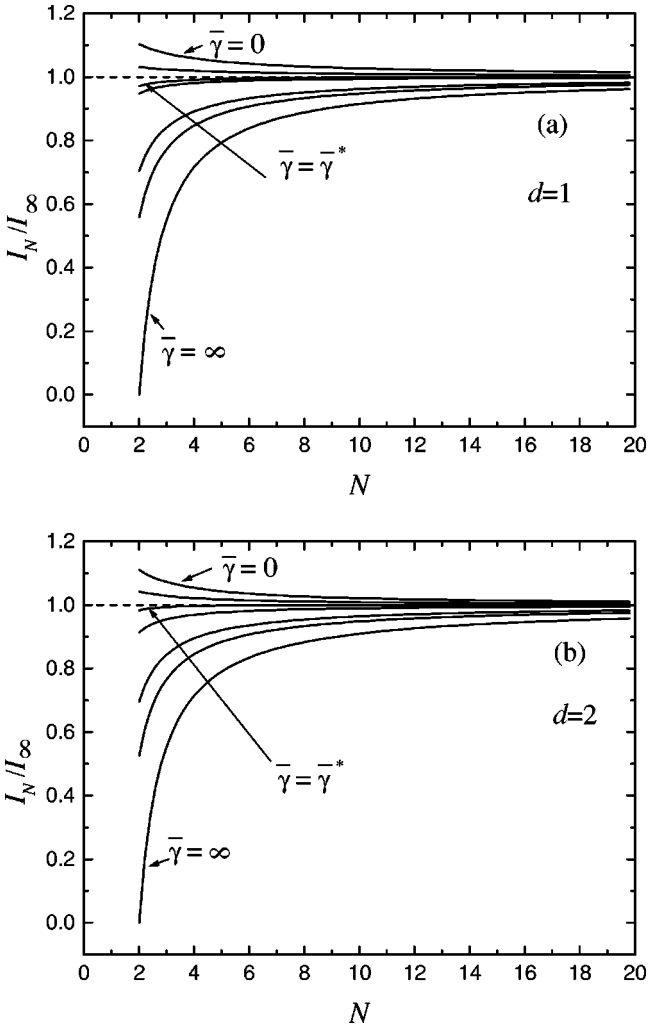

FIG. 2. The ratio I_N/I_∞ as a function of manifold number N for various values of dimensionless interface tension $\bar{\gamma}$, for (a) 2D stacks of semiflexible polymers ($d=1$) and (b) 3D stacks of membranes ($d=2$). From top to bottom, the values of $\bar{\gamma}$ values are 0, $0.5\bar{\gamma}^*$, $1\bar{\gamma}^*$, 1, $5\bar{\gamma}^*$, $10\bar{\gamma}^*$, and ∞. Note that, for the dimensionless interfacial tension $\approx\bar{\gamma}^*$, the average stack period, Eq. (2.11), is nearly independent of the number of the manifolds N (see the end of Sec. II for discussions of this feature).

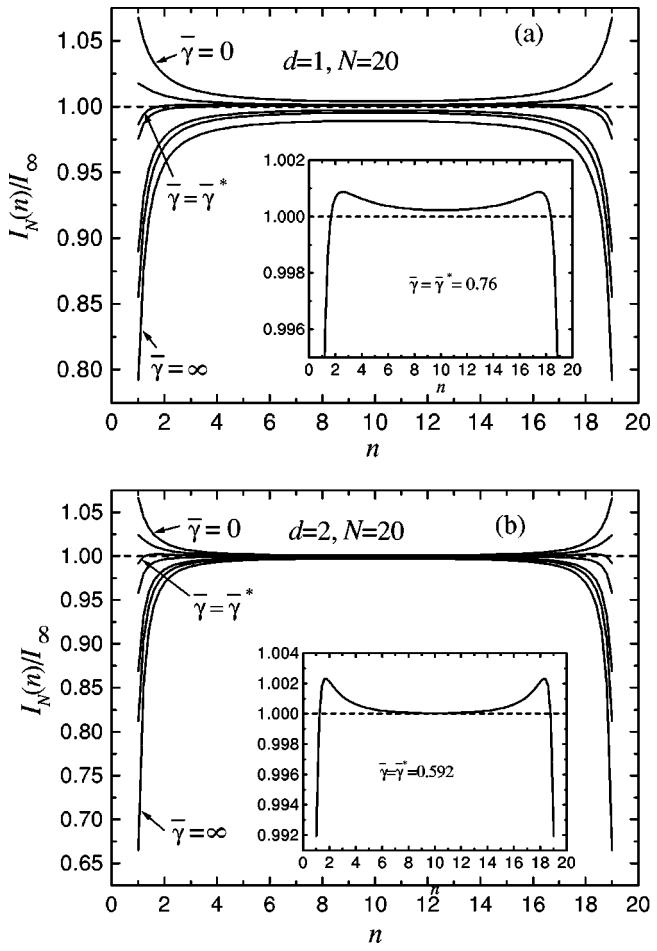

FIG. 3. The ratio $I_N(n)/I_\infty$ as a function of n in a $N=20$-manifold stack, for various values of the dimensionless surface tension $\bar{\gamma}$. (a) 2D stacks of semiflexible polymers ($d=1$) and (b) 3D stacks of membranes ($d=2$). From top to bottom, the values of $\bar{\gamma}$ values are 0, $0.5\bar{\gamma}^*$, $1\bar{\gamma}^*$, 1, $5\bar{\gamma}^*$, $10\bar{\gamma}^*$, and ∞. The inset shows that the interlayer distances, Eq. (2.10), become nearly uniform for the dimensionless interfacial tension $\approx\bar{\gamma}^*$ (see the end of Sec. II for discussions of this feature).

From Fig. 3 and Eq. (2.10), we see that, in a range of small values of $\bar{\gamma}$, the local spacings $a_N(n)$ are actually *bigger* than the bulk period a_∞, in accord with the aforementioned behavior of the average stack period a_N. This feature is a manifestation of our reverse VPP effect [see the Introduction and Fig. 1(c)]. In fact, in Fig. 3, only for the values of $\bar{\gamma}$ above a certain threshold, the interlayer spacings $a_N(n)$ are all *smaller* than a_∞. This feature is the signature of the ordinary VPP effect [see the Introduction and Fig. 1(b)]. We discuss these effects in more detail later on in this section. Here, we stress that our results above have well defined, finite values in the limits of zero and infinite surface tension, $\bar{\gamma}=0$ and $\bar{\gamma}=\infty$, as detailed in Appendix A [see Eqs. (A28)–(A33)]. We stress that for $\bar{\gamma}\to 0$, the function $Z(R)$ in Eq. (2.17) has well defined limit, $Z(R)\to Z_0(R)$, with

$$Z_0(R)=-R^3. \tag{2.19}$$

Likewise, for $\bar{\gamma}\to\infty$, $Z(R)\to Z_\infty(R)$ with

$$Z_\infty(R)=+R^2. \tag{2.20}$$

For 3D smectic stacks of membranes ($d=2$), the integrals in Eqs. (2.15) and (2.16) can be calculated exactly in the limits $\bar{\gamma}=0$ and $\bar{\gamma}=\infty$ (see Appendix A). We obtain

$$I_N(d=2,\bar{\gamma}=0)=\frac{\pi}{2(N-1)}\left[\cot\left(\frac{\pi}{4N}\right)-1\right] \tag{2.21}$$

and

$$I_N(d=2,\bar{\gamma}=\infty)=\frac{\pi}{2(N-1)}\left[\cot\left(\frac{\pi}{4(N-1)}\right)-1\right]. \tag{2.22}$$

We also find, for the intermembrane distances in Eq. (2.13),

$$I_N(n,d=2,\bar{\gamma}=0)=\frac{\pi}{2N}\left[\cot\left(\frac{\pi}{4N}\right)-\frac{1}{2}\cot\left(\frac{\pi}{4N}+\frac{n\pi}{N}\right)-\frac{1}{2}\cot\left(\frac{\pi}{4N}-\frac{n\pi}{N}\right)\right] \tag{2.23}$$

and

$$I_N(n,d=2,\bar{\gamma}=\infty)=\frac{\pi}{2(N-1)}\left[\cot\left(\frac{\pi}{4(N-1)}\right)+\frac{1}{2}\cot\left(\frac{\pi}{4(N-1)}+\frac{(n-\frac{1}{2})\pi}{(N-1)}\right)+\frac{1}{2}\cot\left(\frac{\pi}{4(N-1)}-\frac{(n-\frac{1}{2})\pi}{(N-1)}\right)\right]. \tag{2.24}$$

To elucidate the physical phenomena implied by these results, we consider them in several practically interesting limits discussed in the following.

In practice, the number of the manifolds in smectic stacks is often large, $N\gg 1$. It is thus interesting to see the behavior of local smectic spacings $a_N(n)$ in *semi-infinite* smectic liquid crystals, i.e., to consider $a_N(n)$ for a fixed n in the limit $N\to\infty$. In this limit, from Eq. (2.10),

$$a_\infty(n,\gamma)=a_\infty+A'_d\,\Delta(n,d,\bar{\gamma}) \tag{2.25}$$

with

$$\Delta(n,d,\bar{\gamma})=I_\infty(n,d,\bar{\gamma})-I_\infty(d)=\int_0^1 dR\,\frac{(1-R)^{d/2-1}}{R^{d/4}}\,\frac{Z(R,\bar{\gamma})}{2R^2}(R-1)R^{2(n-1)}. \tag{2.26}$$

For $n \gg 1$, we find the asymptotic expansion of Eq. (2.26),

$$\Delta(n,d,\bar{\gamma}) = \frac{1-\bar{\gamma}}{1+\bar{\gamma}} \frac{\Gamma(1+d/2)}{2^{2+d/2}} \frac{1}{n^{1+d/2}} + \cdots . \quad (2.27)$$

Note that the asymptotic power law tail of $a_\infty(n,\gamma) - a_\infty \sim \Delta(n,\bar{\gamma})$ in Eq. (2.27) changes sign as $\bar{\gamma} = \gamma/\delta\gamma$ crosses 1. Furthermore, for 3D stacks of membranes ($d=2$), we can calculate $\Delta(n,d,\bar{\gamma})$ analytically for $\bar{\gamma} = 0,1$, and ∞. We obtain

$$\Delta(n,d=2,\bar{\gamma}=0) = \frac{1}{8(n-1/4)(n+1/4)} = +\frac{1}{8n^2} + O\left(\frac{1}{n^3}\right),$$

$$\Delta(n,d=2,\bar{\gamma}=1) = -\frac{1}{32n(n-1/2)(n-1/4)} = -\frac{1}{32n^3} + O\left(\frac{1}{n^4}\right),$$

$$\Delta(n,d=2,\bar{\gamma}=\infty) = -\frac{1}{8(n-3/4)(n-1/4)} = -\frac{1}{8n^2} + O\left(\frac{1}{n^3}\right). \quad (2.28)$$

Note that, from Eqs. (2.28) and (2.25), there is a simple relation between semi-infinite system with infinite and zero surface tension γ,

$$a_\infty(n+\tfrac{1}{2},\gamma=\infty) - a_\infty = -[a_\infty(n,\gamma=0) - a_\infty].$$

The results in Eq. (2.28) also manifest a qualitative change of the smectic spacings as $\bar{\gamma} = \gamma/\delta\gamma$ crosses 1. For values of $\bar{\gamma}$ other than 0, 1, and ∞, one can obtain only numerical results for $I_\infty(n,d,\bar{\gamma}) = I_\infty(d) + \Delta(n,d,\bar{\gamma})$, see Fig. 4. Overall, this figure and Eqs. (2.25)–(2.28) evidence the existence of the low- and high-$\bar{\gamma}$ regimes, characterized by interlayer spacings bigger (for the low-$\bar{\gamma}$ regime) or smaller (for the high-$\bar{\gamma}$) than the bulk interlayer spacing a_∞. We anticipate here that the low-$\bar{\gamma}$ regime is directly related to the reverse VPP effect [see the Introduction and Fig. 1(c)]. Likewise, the high-$\bar{\gamma}$ regime is directly related to the ordinary VPP effect in Fig. 1(b). We elucidate the physical nature of these two regimes in the following.

Next, let us consider the case of a large but finite smectic stack with many manifolds, $N \gg 1$. In this limit, $I_N(d,\bar{\gamma})$ in Eq. (2.11) for the average smectic period can be asymptotically expanded,

$$I_N(d,\bar{\gamma}) = I_\infty(d) + \frac{C_1(d,\bar{\gamma})}{N} + \frac{C_{d/2+1}(d,\bar{\gamma})}{N^{d/2+1}} + \cdots , \quad (2.29)$$

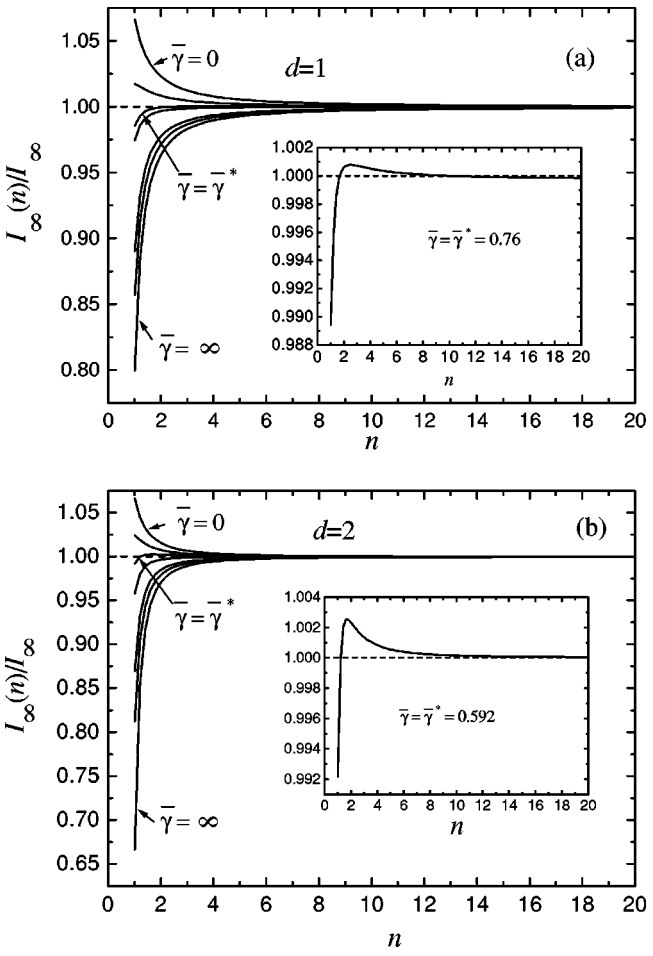

FIG. 4. The ratio $I_\infty(n)/I_\infty$ as the function n, in a semi-infinite manifolds stack ($N=\infty$), for various values of the dimensionless surface tension $\bar{\gamma}$. (a) 2D stacks of semiflexible polymers ($d=1$) and (b) 3D stacks of membranes ($d=2$). From top to bottom, the values of $\bar{\gamma}$ are 0, $0.5\bar{\gamma}^*$, $1\bar{\gamma}^*$, 1, $5\bar{\gamma}^*$, $10\bar{\gamma}^*$, and ∞. The inset shows that interlayer distances, Eq. (2.10), become nearly uniform for the dimensionless interfacial tension $\approx \bar{\gamma}^*$ (see the end of Sec. II for discussions of this feature).

where

$$C_1(d,\bar{\gamma}) = -\int_0^1 dR \, \frac{(1-R)^{d/2-1}}{R^{d/4+2}} \, \frac{Z(R,\bar{\gamma})}{R+1} \quad (2.30)$$

and

$$C_{d/2+1}(d,\bar{\gamma}) = -\int_0^\infty dx \frac{e^{-x}}{1-\left(\frac{\bar{\gamma}-1}{\bar{\gamma}+1}\right)^2 e^{-x}} \times \left[\left(\frac{\bar{\gamma}-1}{\bar{\gamma}+1}\right)^2 x^{d/2} + x^{d/2-1}\left(\frac{\bar{\gamma}-1}{\bar{\gamma}+1}\right) \times \left(\left\{\frac{\bar{\gamma}-1}{\bar{\gamma}+1}\right\}^2 - 1\right)\right]. \quad (2.31)$$

For 3D stacks of membranes ($d=2$), $C_1(d,\bar{\gamma})$ in Eq. (2.30) can be calculated analytically,

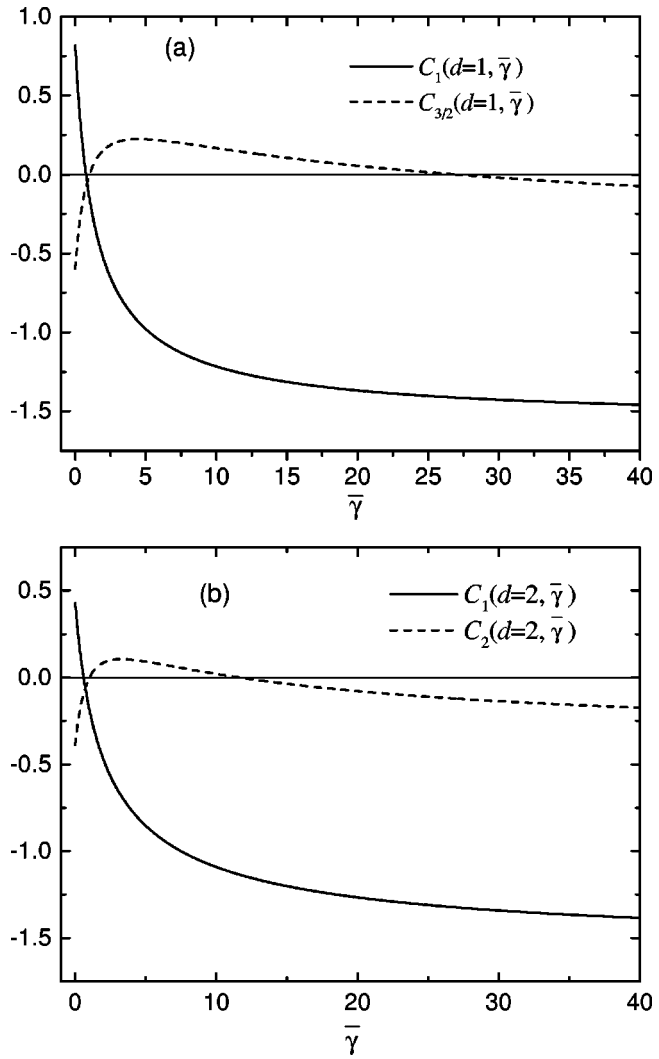

FIG. 5. $C_1(d,\bar{\gamma})$ and $C_{d/2+1}(d,\bar{\gamma})$ as functions of $\bar{\gamma}$ for (a) 2D stacks of semiflexible polymers ($d=1$) and (b) 3D stacks of membranes ($d=2$). $C_1(d,\bar{\gamma})$ goes to zero for $\bar{\gamma}\to\bar{\gamma}^*(d)$. For $d=1$, $\bar{\gamma}^*=0.76$; for $d=2$, $\bar{\gamma}^*=0.592$. We note that, for $d=1$, $C_1(d=1,\bar{\gamma}=0)=0.82$, $C_1(d=1,\bar{\gamma}=\infty)=-1.56$, whereas, for $d=2$, $C_1(d=2,\bar{\gamma}=0)=2-\pi/2$, $C_1(d=2,\bar{\gamma}=\infty)=-\pi/2$. These values are in accord with the exact relation $C_1(d,\bar{\gamma}=0)-C_1(d,\bar{\gamma}=\infty)=I_\infty(d)=B(1-d/4,d/2)$, by noting that $I_\infty(d=2)=B(1/2,1)=2$, and $I_\infty(d=1)=B(3/4,1/2)=2.3963$.

$$C_1(d=2,\bar{\gamma})=-\frac{\pi}{2}+2\frac{\ln(1+\bar{\gamma})}{\bar{\gamma}}. \tag{2.32}$$

$C_1(d,\bar{\gamma})$ and $C_{d/2+1}(d,\bar{\gamma})$ as functions of the parameter $\bar{\gamma}$ are given in Fig. 5 for $d=1$ and 2. We find that $C_1(d,\bar{\gamma})$ is *positive* for small γ and changes sign at $\bar{\gamma}=\bar{\gamma}^*(d)$ with $\bar{\gamma}^*\approx 0.76$ for $d=1$, and $\bar{\gamma}^*\approx 0.592$ for $d=2$, see Fig. 5. For $N\gg 1$, from Eqs. (2.11) and (2.29),

$$a_N(\gamma)-a_\infty\approx\frac{\lambda(\gamma)}{N}. \tag{2.33}$$

Here,

$$\lambda(\gamma)=A_d'\ C_1(d,\bar{\gamma}) \tag{2.34}$$

is an important characteristic length, as evidenced in the following. From Eqs. (2.33) and (2.34), for $\bar{\gamma}>\bar{\gamma}^*$, $\lambda(\gamma)<0$ and the average smectic period $a_N(\gamma)$ is smaller than the infinite smectic period a_∞. Physically, this feature emerges due to the suppression of the thermal fluctuations of the manifolds close to the interfaces of the system, which is caused by surface tension of interfaces [as conceptualized in Fig. 1(b)]. Due to it, for the manifolds close to the stack surfaces, the fluctuation contribution to their interlayer spacings $a_N(n,\gamma)$ [the second, bond expansion term in Eq. (2.7)] is smaller than in the bulk. Thus, for large enough surface tension, from Eqs. (2.7) and (2.8), both $a_N(n,\gamma)$ and $a_N(\gamma)$ are *smaller* than the bulk smectic period a_∞ [we recall that b_3 in Eqs. (2.7) and (2.8) is typically negative]. This feature is the signature of the ordinary VPP effect anticipated in the Introduction [see Fig. 1(b)]. On the other side, in the range of small surface tension $\bar{\gamma}<\bar{\gamma}^*$, from Eqs. (2.33) and (2.34), $\lambda(\gamma)>0$, and the average smectic period $a_N(\gamma)$actually exceeds its bulk value a_∞. This feature is the signature of our reverse VPP effect anticipated in the Introduction [see Fig. 1(c)]. As noted therein, this effect can be physically rationalized by considering the $\bar{\gamma}=0$ limit. Then, all manifolds are tensionless, but the surface manifolds (with just one neighbor) are obviously more free to thermally fluctuate than other manifolds (confined by two neighbors). Consequently, for small enough surface tensions, the thermal bond expansion of interlayer spacings [the second bond expansion term in Eq. (2.7)] is bigger for the manifolds close to stack surfaces than for those in the bulk, as evidenced above by our quantitative results for $\bar{\gamma}<\bar{\gamma}^*$. Thus, for small enough surface tension, from Eqs. (2.7) and (2.8), both $a_N(n,\gamma)$ and $a_N(\gamma)$ are *bigger* than the bulk smectic period a_∞, and one has our reverse VPP effect, as depicted in Fig. 1(c).

Thus, by consistently taking into account the discrete, layered character of smectic liquid crystals, and anharmonic phonon effects, the above theory shows that the essence of VPP effects is in spatially nonuniform thermal expansion of smectic interlayer separations. The average period of the whole finite stack can be both smaller (ordinary VPP effect at high enough interfacial tensions) or bigger (a reverse VPP effect at low interfacial tensions), relative to the average period of the corresponding infinite smectic stack, see Fig. 1. Looking at stacks from the *outside*, these two effects show up as if there is an attractive (for the ordinary VPP effect) or repulsive (for the reverse VPP effect) pseudo-Casimir force acting between the two stack interfaces. However, the physics of VPP effects is obscured by schematically invoking Casimir-like forces. Rather, the ordinary and the reverse VPP effects are to be *both* characterized as anharmonic effects caused by a spatially nonuniform thermal expansion of smectic interlayer distances. Interlayer distances close to stack surfaces expand less (more) for the ordinary (reverse) VPP effect than the interlayer distances deep in the stack, see Figs. 1(a)–1(c). The reverse VPP prevails at low interface

tensions simply because the membrane at the top of the stack is then more free to fluctuate than membranes in the bulk. Therefore, for low interface tensions, thermal expansion of interlayer distances (an anharmonic fluctuation effect) is bigger close to stack interfaces than in the stack center, where interlayer spacing is close to its thermodynamic limit a_∞. Thus, at low surface tensions, the average period of the whole finite stack, a_N, is bigger than a_∞ and one has the reverse VPP effect in Fig. 1(c). By increasing interface tension above a threshold value, fluctuations of the membrane at the stack surface become suppressed, and the ordinary VPP effect in Fig. 1(b) prevails. For this effect too, the spatial nonuniformity of thermal expansion plays the essential role: Here, the thermal expansion of interlayer distances (the *same* anharmonic fluctuation effect) is smaller close to stack interfaces than in the stack center, where interlayer spacing is close to its thermodynamic limit a_∞. Thus, at high enough surface tensions, the average period of the whole finite stack, a_N, is smaller than a_∞. Previous Podgornik-Parsegian theory of VPP [14] obscures the essential role played by the nonuniformity of smectic interlayer distances, by simply assuming that they are uniform throughout the system. Within this assumption, the difference between the average period of the whole finite stack a_N and its bulk value a_∞ is attributed to an extra pressure ΔP (pseudo-Casimir pressure) acting on the smectic stack interfaces in addition to the osmotic pressure. Within this interpretation, the average period $a_N(d,\gamma)$ of a finite stack can be written by using the infinite stack equation of state, $a_\infty = f_\infty(P)$, with P replaced by $P+\Delta P$,

$$\begin{aligned} a_N(\gamma) &= f_N(P) \\ &= f_\infty(P+\Delta P) \\ &\approx f_\infty(P) + \frac{\partial f_\infty(P)}{\partial P}\Delta P + \cdots \\ &= a_\infty + \frac{\partial a_\infty}{\partial P}\Delta P + \cdots . \end{aligned} \tag{2.35}$$

Thus, for $N \gg 1$, the extra pressure is given by

$$\Delta P \approx \frac{a_N(\gamma) - a_\infty}{\partial a_\infty / \partial P}. \tag{2.36}$$

From Eqs. (2.36), (2.33) and (2.34) we find

$$\Delta P \approx \frac{\lambda(\gamma)}{N a_\infty} B_{sm} \approx \frac{\lambda(\gamma)}{L_z} B_{sm} \tag{2.37}$$

with $B_{sm} = -a(\partial P/\partial a)$ being the usual smectic compressibility modulus (see, e.g., Ref. [11]) and $L_z \approx N a_\infty$ being the height of the stack. For $\bar{\gamma} > \bar{\gamma}^*$, the extra (Casimir) pressure ΔP is positive for the ordinary VPP effect, as if the stack interfaces would be attracting each other. Conversely, for $\bar{\gamma} < \bar{\gamma}^*$, ΔP is negative for the reverse VPP effect, as if there is a repulsive pseudo-Casimir force between the stack interfaces.

However, the above schematic interpretation of the VPP effects in terms of the pseudo-Casimir pressure obscures the real nature of these effects, namely, the essential role played by the nonuniform thermal expansion of the smectic interlayer distances. Indeed, a true extra osmotic pressure ΔP would induce a *uniform* strain $a_N(n) - a_\infty$ throughout the bulk, that would be, from Eq. (2.37), proportional to $\Delta P \sim 1/N$. However, this is *not* the case, as evidenced in Fig. 3. For example, close to the center of the stack ($n \approx N/2$), we find

$$a_N(n_{mid}, \gamma) - a_\infty \sim 1/N^{1+d/2} \ll 1/N \tag{2.38}$$

with $n_{mid} \approx N/2$ [much similar to the result in Eq. (2.27)]. In fact, the leading $1/N$ contribution to the difference between the average stack period a_N and its bulk value a_∞ comes from the regions that are close to the two stack interfaces. To see this, let us rewrite Eq. (2.6) as

$$a_N(\gamma) - a_\infty = \frac{\sum_{n=1}^{N-1} [a_N(n,\gamma) - a_\infty]}{N-1}. \tag{2.39}$$

For $N \gg 1$, the sum in Eq. (2.39) can be asymptotically evaluated by using the semi-infinite smectic spacing profile $a_\infty(n)$, and by recalling that *both* smectic interfaces contribute to the sum. Thus, for $N \gg 1$,

$$a_N(\gamma) - a_\infty \approx \frac{\lambda(\gamma)}{N} \tag{2.40}$$

with

$$\lambda(\gamma) = 2\sum_{n=1}^{\infty} [a_\infty(n,\gamma) - a_\infty] \tag{2.41}$$

exactly. In Eq. (2.41), the factor of 2 emerges simply because both stack interfaces contribute to the sum in Eq. (2.39). In the semi-infinite system, $a_\infty(n) - a_\infty \sim 1/n^{1+d/2} \ll 1/n$ and the sum in Eq. (2.41) is finite, suggesting, using Eq. (2.40), that the difference $a_N - a_\infty$ is dominated by the behavior of the smectic spacings close to the stack surfaces. We note that our previous one-loop results also reflect this exact asymptotic behavior in Eqs. (2.40) and (2.41). In fact, the one-loop result for $\lambda(\gamma)$ in Eq. (2.34) can be shown to be consistent with Eq. (2.41), by noting that $\Delta(n,\bar{\gamma})$ in Eq. (2.26) is actually related to $C_1(\bar{\gamma})$ in Eq. (2.30) via the identity $C_1(\bar{\gamma}) = 2\Sigma_{n=1}^{\infty}\Delta(n,\bar{\gamma})$. The one-loop result shows that the characteristic length $\lambda(\gamma)$ is intimately related to the thermal expansion of the stack. Indeed, using Eq. (2.12), $A_d' = (a_\infty - r_0)/I_\infty(d)$. Thus, using Eq. (2.34),

$$\lambda(\gamma) = \frac{C_1(d,\bar{\gamma})}{I_\infty(d)}(a_\infty - r_0) \tag{2.42}$$

and thus

$$a_N(\gamma)-a_\infty=\frac{C_1(d,\bar{\gamma})}{I_\infty(d)}\,\frac{a_\infty-r_0}{N} \tag{2.43}$$

for $N\gg 1$, to one-loop order. More generally, for any N, from Eqs. (2.11) and (2.12),

$$a_N(\gamma)-a_\infty=\left(\frac{I_N(d,\bar{\gamma})}{I_\infty(d)}-1\right)(a_\infty-r_0) \tag{2.44}$$

to one-loop order. We recall that the ratio $I_N(\bar{\gamma},d)/I_\infty(d)$ here is given by Fig. 2, for $d=1$ and 2, whereas $I_\infty(d)=B(1-d/4,d/2)$, so $I_\infty(d=2)=2$ and $I_\infty(d=1)\cong 2.3936$. Equations (2.42)–(2.44) manifestly show that the strength of the finite-size effect of the surface tension γ crucially depends on the magnitude of $a_\infty-r_0$, i.e., the thermal expansion of the smectic bulk period a_∞ away from r_0 minimizing the net intermanifold potential $V_{net}(r)=V(r)+Pr$.

To exemplify our results, let us consider the system studied in the experiments of Katsaras [17], aimed to investigate the VPP phenomenon (see Sec. I). He studied multilamellar L_α phase of bilayer DMPC fluid membranes ($d=2$). The bare intermembrane potential for these systems of neutral lipids is the sum of van der Waals attraction and hydration force repulsion,

$$V(r)\approx-\frac{H}{l^2}+P_h\lambda_h e^{-l/\lambda_h}, \tag{2.45}$$

with $l=r-a_{min}=h_{n+1}-h_n-a_{min}$ being the surface-to-surface intermembrane distance (water gap), a_{min} being the membrane thickness (representing the smallest possible smectic phase period). Equation (2.45) applies for l up to $\approx a_{min}$. Here, for DMPC membranes, the material's parameters in the potential Eq. (2.45) are, after Ref. [19], $H=W_H/12\pi=0.0483k_BT$ ($T=300$ K), $\lambda_h=0.191$ nm, $P_h=1.32\times10^8$ J/m^3. For DMPC lipid bilayers, $a_{min}\approx 4.4$ nm, whereas the membrane bending rigidity constant $\kappa\approx 12.8k_BT$. Let us consider the case with zero osmotic pressure, $P=0$, so that r_0 is obtained by minimizing $V(r)$ in Eq. (2.45) over $l=r-a_{min}$. This yields the equation $P_h\lambda_h^3/2H=(\lambda_h/l)^3\exp(l/\lambda_h)$, yielding potential minimum at $l_0=r_0-a_{min}\approx 6.5\lambda_h\approx 1.243$ nm, i.e., $r_0=5.64$ nm. Due to thermal fluctuations, the stack average period expands away from r_0 to the true equilibrium value a_N. The magnitude of this thermal expansion, for the infinite stack ($N=\infty$), can be estimated by Eqs. (2.12), (2.18), and (2.45), to be, for $P=0$,

$$a_\infty-r_0=A'_{d=2}I_\infty(d=2)=\frac{l_0}{2}\,\frac{\left[1-12\left(\frac{\lambda_h}{l_0}\right)^2\right]\left(\frac{l_0}{\lambda_h}\right)^{1/2}}{\left(1-3\frac{\lambda_h}{l_0}\right)^{3/2}}\,\frac{k_BT}{2\pi\sqrt{2\kappa H}}. \tag{2.46}$$

With $l_0/\lambda_h\approx 6.5$ as found above, one finds for DMPC, $a_\infty-r_0\approx 0.411$ nm for the thermal period expansion in the bulk ($N=\infty$). This estimate can be now easily combined with Eq. (2.43) to see the conditions needed for the finite-size VPP effects to be observed in the experiments of Katsaras with L_α phases of DMPC membranes ($d=2$). For this purpose, we recall that here $d=2$, and Eq. (2.43) is to be used with $I_\infty(d=2)=2$, whereas $C_1(\bar{\gamma},d=2)$ is given by the simple closed formula in Eq. (2.32), depicted in Fig. 5(b) versus $\bar{\gamma}=\gamma/\delta\gamma$. We stress that the values of C_1 are confined in a *finite* range between the values $C_1=2-\pi/2>0$ reached for $\bar{\gamma}\to 0$, and $C_1=-\pi/2<0$ reached for $\bar{\gamma}\to\infty$, [see, also, Fig. 5(b)]. With this range in mind, and by recalling that $a_\infty-r_0\approx 0.41$ nm as found above, we see that Eq. (2.43) indicates that $|a_N(\gamma)-a_\infty|$ is less than 0.03 nm (the maximum accuracy in the experiments of Katsaras [17]) already for $N>10$ membranes, and for *whatever* value of the surface tension γ. In fact, for $N=600$–1800 membranes, as in the investigation of Katsaras [17], the magnitude of the VPP finite-size effect in our Eq. (2.43) is $|a_N-a_\infty|\sim 3\times10^{-5}$ nm, far below the experimental resolution. Our results thus explain the enigmatic absence of noticeable VPP effects in these experiments (see Sec. I). As $|a_N-a_\infty|\sim(a_\infty-r_0)/N$, the primary limiting factor for the VPP phenomenon is a typically small value of the stack period thermal expansion $a_\infty-r_0$. From our results, the best systems to study VPP effects are relatively small stacks, with $N=10$–20 membranes. It is interesting to note that membrane stacks are in practice frequently asymmetric. For example, in the recent experiment of Vogel *et al.* [28], one membrane is supported on a solid substrate (corresponding to $\gamma=\infty$ limit), while the other one was free to fluctuate in water [as in Fig. 1(e), corresponding to $\gamma=0$]. We are not going to pursue here a detailed discussion of asymmetric stacks. We just note that, by a reasoning similar to that yielding Eq. (2.30), for asymmetric stacks, one also has the exact asymptotic formula

$$a_N-a_\infty=\frac{\lambda}{N}+\cdots. \tag{2.47}$$

Here $\lambda=(\lambda_1+\lambda_2)/2$, with, to one-loop order, $\lambda_i=A'_dC_1(\bar{\gamma}_i,d)=(a_\infty-r_0)C_1(\bar{\gamma}_i,d)/I_\infty(d)$, $(i=1,2)$, where γ_1 and γ_2 are interfacial tensions of the upper and lower interfaces of the stack.

Thus, the finite-size VPP effects are shown here to be significantly limited by the size N of the stack, and by the practically modest thermal expansion effects. Small stacks with 10–20 manifolds (such as the thin smectic films [26]) would be best to use to investigate these effects in future experiments. We note that the validity of the one-loop theory pursued in this section is, in part, only qualitative, if this theory is to be applied (at room temperature) to strongly anharmonic potentials with sharp minima, such as the potential in Eq. (2.45). For this potential, at room temperature, two- and higher-loop corrections are comparable to the one-loop result. For this reason, in Sec. III we consider in detail systems with strongly anharmonic potentials, with sharp nonanalytic minima. Interestingly, there we find that VPP effects in these entropically dominated systems are both qualitatively and quantitatively similar to those found in this

section, and can be understood by the one-loop theory applied to effective (coarse-grained) potentials acting between manifolds, see Sec. III. Finally, we stress that the analytic results discussed in this section are presented in the continuum limit $\Delta x \to 0$, with Δx being the manifold short-distance cutoff [e.g., for membranes, Δx = lipid molecule size]. In fact, the stack model has a finite continuum limit for $d<4$, and the corrections due to a finite molecular size Δx are small in practical situations [see the end of Appendix A].

Finally, we comment on the magnitude of the characteristic value of the interface tension separating the regimes of the reverse and the ordinary VPP effects. From the results of this section, the crossover between the two regimes occurs for the interface tension $\gamma^* = \bar{\gamma}^* \cdot \delta\gamma = \bar{\gamma}^* \sqrt{\kappa b_2} = O(1)\sqrt{\kappa b_2}$. [See Eqs. (2.13) and (2.14), and our results for $\bar{\gamma}^*$.] For γ smaller (bigger) than γ^*, a_N is bigger (smaller) than a_∞, and the reverse (ordinary) VPP effect prevails. A special feature of the finite smectic stacks with tensions $\gamma \approx \gamma^*$ is that they are nearly uniform [see Figs. 2–4, and recall Eqs. (2.10) and (2.11)]. It is not an accident that this happens for interface tension $\approx \delta\gamma = \sqrt{\kappa b_2}$. In fact, $\delta\gamma = \sqrt{\kappa b_2} = \sqrt{K_{sm} B_{sm}}$ is the well known smectic ''elastic'' surface tension of the interface of semi-infinite smectic liquid crystals [12,13]. Furthermore, it has been recently shown, in our work [12], that applying interface tensions $\approx \delta\gamma$ makes finite smectic stack nearly uniform for *any N*. This is because for $\gamma \approx \gamma^* \approx \delta\gamma$, finite stacks behave as subsystems of infinite, spatially uniform smectic stacks [such as that in Fig. 1(a)]. Thus, for $\gamma \approx \gamma^*$, one has $a_N \approx a_\infty$, as evidenced in Fig. 2 [here, recall Eq. (2.11)]. We direct readers to Ref. [12] for details of this interesting effect in finite smectic stacks with interfacial tensions $\gamma \approx \delta\gamma$.

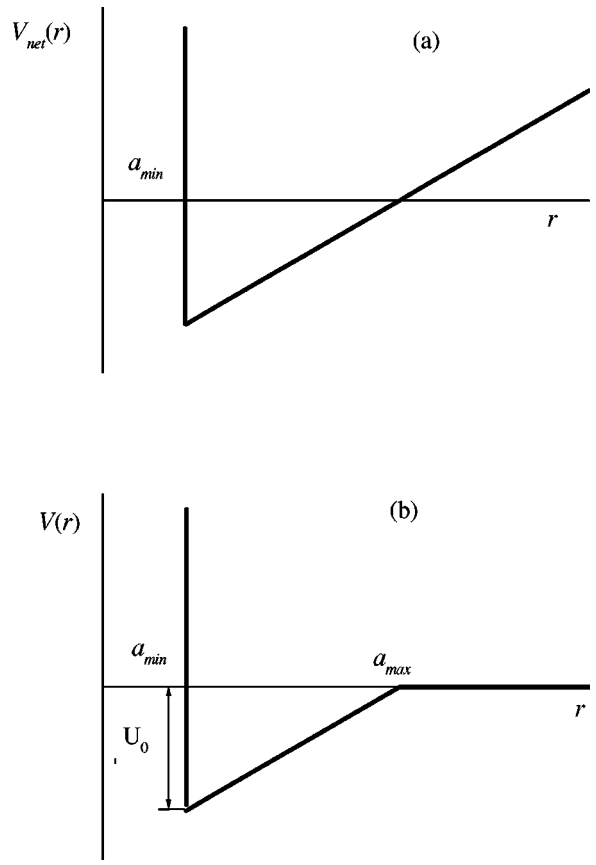

FIG. 6. (a) The net potential for sterically stabilized systems, $V_{net}(r) = V_{hc}(r) + Pr$. (b) A model potential for bound stacks of manifolds. For $P = U_0/(a_{max} - a_{min})$, potentials in (a) and (b) are the same for $r < a_{max}$.

III. FINITE-SIZE EFFECTS IN ENTROPICALLY DOMINATED SMECTIC STACKS

In this section, we consider finite-size effects in the stacks of manifolds interacting through strongly anharmonic potentials, with nonanalytic minima. Typical examples are sterically stabilized phases of manifolds interacting through the hard-core potential of the form

$$V_{hc}(r) = \begin{cases} 0, & r > a_{min} \\ \infty, & r < a_{min}. \end{cases} \tag{3.1}$$

Here, as in Sec. II, $r = h_{n+1}(\mathbf{x}) - h_n(\mathbf{x})$, and a_{min} is the manifold thickness setting the smallest possible period of the smectic phase. The net potential $V_{net}(r) = V(r) + Pr$ has a *nonanalytic* minimum at $r = a_{min}$ [see Fig. 6(a)] and the perturbation theory of Sec. II can not be directly applied to these smectic systems of great practical and theoretical interest [2,10–12,21–23]. As pointed out for the first time by Helfrich [10], the equation of state in these sterically stabilized systems is purely entropic in character of the form [11]

$$a_\infty = \beta_\infty(d) \frac{(k_B T)^{4/(4+d)}}{\kappa^{d/(4+d)} P^{(4-d)/(4+d)}} + a_{min} \tag{3.2}$$

in the thermodynamic limit $N \to \infty$. Here, for 2D smectic phases of semiflexible polymers ($d=1$), $\beta_\infty(d=1) \cong 0.611$ (as recently found by us in Ref. [11]), whereas for 3D smectic phase of membranes ($d=2$), $\beta_\infty(d=2) \cong 0.595$ (see Refs. [22,23], and the discussion in the following). Highly entropic character of the equation of state (3.2) is physically described by introducing the concept of the effective repulsive potential, of the form

$$V_{eff}(r) = \frac{4-d}{2d} \alpha_\infty(d) \frac{(k_B T)^{4/(4-d)}}{\kappa^{d/(4-d)} (r - a_{min})^{2d/(4-d)}} \tag{3.3}$$

with $\alpha_\infty(d, \gamma) = [\beta_\infty(d, \gamma)]^{(4+d)/(4-d)}$, see Ref. [11]. Minimization of the effective net potential $V_{net}(r) = V_{eff}(r) + Pr$ gives the steric equation of state (3.2). We stress that the above results apply for $d<4$, when the free semiflexible manifolds are thermally rough. Then, also, the stack model has perfect continuum limit $\Delta x \to 0$, with Δx, for example, the lipid molecule size, in the application to lamellar phases of membranes ($d=2$), see Appendix A.

In the following we will study the finite-size effect in these system, by means of an exact scaling analysis and Monte Carlo simulations. It will be shown that these results may be rationalized by the analytic results of Sec. II, provided one assumes that manifolds interact by effective

coarse-grained potentials such as that in Eq. (3.3). Besides the direct interest for the unbound stack of manifolds [with $a_\infty \to \infty$ for $P \to 0$, as in Eq. (3.2)], our results will shine more light also on the behavior of *bound* stacks of manifolds, in the situation in which potentials have analytic but sharp minima, yielding strong anharmonic effects of thermal fluctuations. When the intermembrane distance fluctuates far away from the sharp analytic or nonanalytic minimum of the potential, such as in Fig. 6(b), analytic details of the potential close to its minimum do not matter. For example, the sharp nonanalytic potential minimum in Fig. 6(b) can be slightly rounded and replaced by a sharp analytic minimum. Such a change cannot affect significantly fluctuations of intermembrane distance, if their magnitude is bigger than the size of the rounded range. Such situations are frequently realized in practice at room temperature (see the end of Sec. II). Intermembrane distance may strongly fluctuate far away from the sharp minimum of the intermembrane potential. The sum of the full perturbation theory is divergent in such situations, indicating that the fluctuations behave as in potentials with sharp nonanalytic minima, such as the potential depicted in Fig. 6(b). This potential has a finite range a_{max}, but for $r < a_{max}$, it has exactly the same shape as the net potential for the sterically stabilized systems, $V_{net}(r) = V_{hc}(r) + Pr$, Fig. 6(a), provided $P = U_o/(a_{max} - a_{min})$, with U_0 being the depth of the binding potential in Fig. 6(b). Away from the unbinding transition ($a_\infty - a_{min} \ll a_{max} - a_{min}$), the binding potential in Fig. 6(b) should yield the same physics as the net potential of the unbound sterically stabilized systems under a nonzero osmotic pressure, Fig. 6(a). Thus, by studying it, one can learn more also on the aforementioned strong entropic effects in the bound stack of manifolds.

We proceed by considering the stack Hamiltonian, Eqs. (2.1)–(2.4), with purely hard-core intermanifold interaction potential in Eq. (3.1). We will use the fact that the stack model for $d < 4$ has finite continuum limit $\Delta x \to 0$ (see Appendix A, and, also, Ref. [11]). The $\mathbf{x}$ coordinate can be thus treated as continuous, and the stack model can be thus freely rescaled for the physically interesting manifolds with $d = 1$ (semiflexible polymers) or $d = 2$ (membranes). Here, it is convenient to do this rescaling as follows:

$$\mathbf{x} = Z_x \mathbf{x}', \quad h_n(\mathbf{x}) = Z_h h_n'(\mathbf{x}') + n a_{min}. \tag{3.4}$$

This transformation maps the stack model with $a_{min} \neq 0$, into an isomorphic model with $a_{min} = 0$, and the rescaled parameters

$$P' = P Z_x^d Z_h, \quad \kappa' = \kappa Z_h^2 Z_x^{d-4}, \quad \gamma' = \gamma Z_h^2 Z_x^{d-2}. \tag{3.5}$$

From Eq. (3.4), we have, for the average intermanifold spacings,

$$\begin{aligned} a_N(n,\gamma) &= \langle h_{n+1}(\mathbf{x}) - h_n(\mathbf{x}) \rangle_{P,\kappa,\gamma,a_{min}} \\ &= Z_h \langle h_{n+1}'(\mathbf{x}') - h_n'(\mathbf{x}') \rangle_{P',\kappa',\gamma',a_{min}=0} + a_{min}. \end{aligned} \tag{3.6}$$

It is convenient to fix the rescaling constants Z_x and Z_h by the conditions

$$\overline{P}' = \frac{P'}{k_B T} = 1, \quad \overline{\kappa}' = \frac{\kappa'}{k_B T} = 1, \tag{3.7}$$

yielding, from Eq. (3.5),

$$Z_x = \frac{(k_B T)^{1/(4+d)} \kappa^{1/(4+d)}}{P^{2/(4+d)}}, \quad Z_h = \frac{(k_B T)^{4/(4+d)}}{\kappa^{d/(4+d)} P^{(4-d)/(4+d)}}, \tag{3.8}$$

and from Eq. (3.6),

$$a_N(n,\gamma) = \beta_N(n,d,\overline{\gamma}') \frac{(k_B T)^{4/(4+d)}}{\kappa^{d/(4+d)} P^{(4-d)/(4+d)}} + a_{min}. \tag{3.9}$$

Here,

$$\beta_N(n,d,\overline{\gamma}') = \langle h_{n+1}'(\mathbf{x}') - h_n'(\mathbf{x}') \rangle_{\overline{P}'=1,\overline{\kappa}'=1,\overline{\gamma}',a_{min}=0} \tag{3.10}$$

is the average done with respect to the rescaled stack Hamiltonian with the reduced parameters $\overline{P}' = 1$, $\overline{\kappa}' = 1$, as in Eq. (3.7), whereas, by using Eqs. (3.8) and (3.5),

$$\overline{\gamma}' = \frac{\gamma'}{k_B T} = \frac{(k_B T)^{2/(4+d)}}{\kappa^{(d+2)/(4+d)} P^{4/(4+d)}} \gamma. \tag{3.11}$$

The reduced rescaled stack Hamiltonian thus has the form

$$\begin{aligned} \frac{H}{k_B T} = \int d^d \mathbf{x}' \Bigg\{ & \sum_{n=1}^{N-1} [(h_{n+1}'(\mathbf{x}') - h_n'(\mathbf{x}')) \\ & + V_{hc}(h_{n+1}'(\mathbf{x}') - h_n'(\mathbf{x}'))] + \sum_{n=1}^{N} \frac{1}{2} \left(\frac{\partial^2 h_n'(\mathbf{x}')}{\partial \mathbf{x}'^2} \right)^2 \\ & + \frac{\overline{\gamma}'}{2} \left[\left(\frac{\partial h_1'(\mathbf{x}')}{\partial \mathbf{x}'} \right)^2 + \left(\frac{\partial h_N'(\mathbf{x}')}{\partial \mathbf{x}'} \right)^2 \right] \Bigg\}. \end{aligned} \tag{3.12}$$

Here, the hard-core potential V_{hc} is as in Eq. (3.1) with $a_{min} = 0$. Notably, the average Eq. (3.10), done with respect to the Hamiltonian in Eq. (3.12), depends only on a single dimensionless parameter $\overline{\gamma}'$ defined in Eq. (3.11). There is a close relationship between $\overline{\gamma}'$ and the dimensionless surface tension $\overline{\gamma} = \gamma/\delta\gamma$ introduced in Sec. II [see Eqs. (2.13) and (2.14)]: From Eq. (2.14), with $b_2 = d^2 V_{eff}/da^2$, and from Eq. (3.3), we find that, for the sterically stabilized smectic liquid crystals,

$$\delta\gamma = \sqrt{\frac{4+d}{4-d}} \alpha_\infty(d) \frac{(k_B T)^{2/(4-d)}}{\kappa^{(d-2)/(4-d)} (a - a_{min})^{4/(4-d)}}. \tag{3.13}$$

From Eqs. (3.13) and (3.2), one also has

$$\delta\gamma = \sqrt{\frac{4+d}{4-d}\frac{1}{\beta_\infty(d)}}\frac{\kappa^{(2+d)/(4+d)}P^{4/(4+d)}}{(k_BT)^{2/(4+d)}}. \quad (3.14)$$

Thus, by using Eqs. (3.14) and (3.11),

$$\overline{\gamma} = \frac{\gamma}{\delta\gamma} = \sqrt{\frac{4+d}{4-d}\beta_\infty(d)}\,\overline{\gamma}'. \quad (3.15)$$

So, the parameter $\overline{\gamma}$ of Sec. II is simply proportional to the parameter $\overline{\gamma}'$ here, which is the single parameter of the rescaled reduced Hamiltonian Eq. (3.12) to be used to find the constants $\beta_N(n,d,\overline{\gamma}')$ by doing the average in Eq. (3.10). These constants are nothing else but average intermanifold spacings for the rescaled reduced Hamiltonian Eq. (3.12). We can thus directly obtain the constants $\beta_N(n,d,\overline{\gamma}')$ by Monte Carlo simulations of the rescaled reduced Hamiltonian Eq. (3.12). Technical details of our simulations are the same as in our previous closely related work, Ref. [11] (see the Appendix therein). As in Sec. II, here we are interested in the average period of the whole stack, Eq. (2.6), which is here, by using Eq. (3.9),

$$a_N(\gamma) = \beta_N(d,\overline{\gamma}')\frac{(k_BT)^{4/(4+d)}}{\kappa^{d/(4+d)}\ P^{(4-d)/(4+d)}} + a_{min} \quad (3.16)$$

with

$$\beta_N(d,\overline{\gamma}') = \frac{\sum_{n=1}^{N-1}\beta_N(n,d,\overline{\gamma}')}{N-1} = \frac{\langle h_N'(\mathbf{x}') - h_1'(\mathbf{x}')\rangle}{N-1}. \quad (3.17)$$

It is enlightening to express the above exact results in a form very similar to that we had in Sec. II: Using Eqs. (3.2), (3.9), and (3.16), we have

$$a_N(n,\gamma) = a_\infty + \frac{(k_BT)^{4/(4+d)}}{\kappa^{d/(4+d)}P^{(4-d)/(4+d)}}[\beta_N(n,d,\overline{\gamma}') - \beta_\infty(d)] \quad (3.18)$$

and

$$a_N(\gamma) = a_\infty + \frac{(k_BT)^{4/(4+d)}}{\kappa^{d/(4+d)}P^{(4-d)/(4+d)}}[\beta_N(d,\overline{\gamma}') - \beta_\infty(d)] \quad (3.19)$$

to be compared with Eqs. (2.10) and (2.11). We also have, using Eqs. (3.16) and (3.2),

$$a_N(\gamma) - a_\infty = \left(\frac{\beta_N(d,\overline{\gamma}')}{\beta_\infty(d)} - 1\right)(a_\infty - a_{min}) \quad (3.20)$$

to be compared with Eq. (2.44). Obviously, the dimensionless constants $\beta_N(d,\overline{\gamma}')$ here play a role similar to that of the dimensionless quantities $I_N(d,\overline{\gamma})$ of Sec. II. This similarity is further amplified by our numerical results for the constants

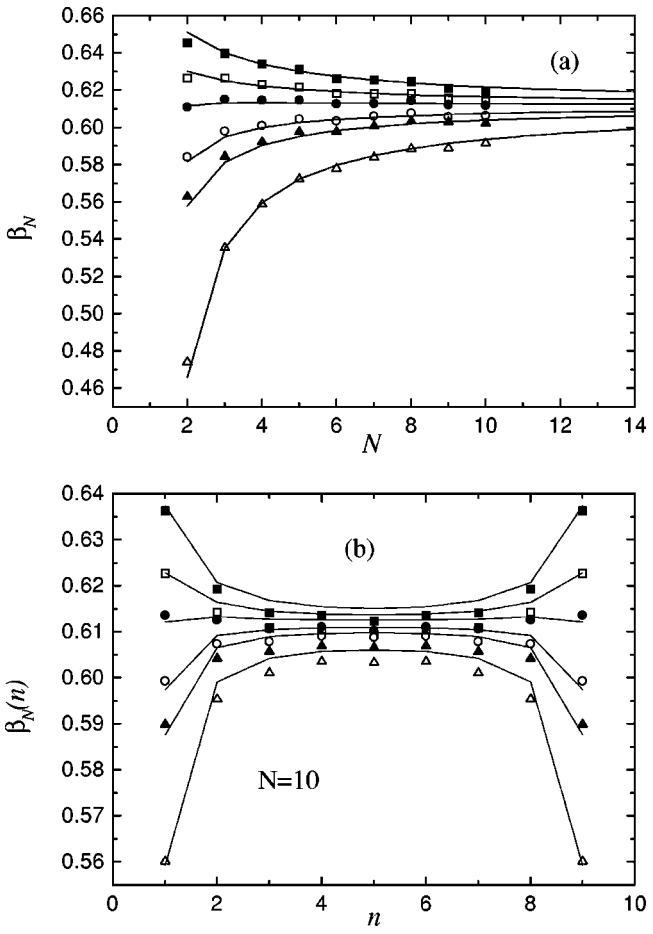

FIG. 7. (a) Monte Carlo simulation results for the universal function $\beta_N(d=1,\overline{\gamma}')$ for 2D stacks of N semiflexible polymers and (b) interlayer spacing universal function $\beta_N(n,d=1,\overline{\gamma}')$ versus n for $N=10$ polymer stack for various values of the surface tension $\overline{\gamma}'=0$, 0.5, 1, 2, 3, and 10 from top to bottom. The data in both (a) and (b) are well fitted by Eqs. (2.10) and (2.11) (solid lines) with $\beta_\infty(d=1)\simeq 0.611$ and $A_d'(d=1)\simeq 0.161$.

$\beta_N(d=1,\overline{\gamma}')$ given in Fig. 7(a), and $\beta_N(n,d=1,\overline{\gamma}')$ in Fig. 7(b), which are all obtained by Monte Carlo simulations of the rescaled model, by calculating the average in Eqs. (3.17) and (3.10). Thus, Fig. 7(a) here clearly corresponds to Fig. 2(a) of Sec. II, yielding [in combination with Eq. (3.20)] the same qualitative message we get in Sec. II: In a range of small tensions $\overline{\gamma}'$, one has the reverse VPP effect [Fig. 1(c)], with $a_N > a_\infty$, as if there are repulsive pseudo-Casimir forces between stack surfaces. And, only for large enough $\overline{\gamma}'$, the ordinary VPP effect [Fig. 1(b)] occurs, with $a_N < a_\infty$, as if there are attractive pseudo-Casimir forces (however, see Sec. II for our criticism of schematically using here the concept of such forces). Local interlayer distances $a_N(n)$ that we find here also behave in a similar way as in Sec. II: Compare Fig. 3(a) of Sec. II with Fig. 7(b) here, both evidencing the crossover from the reverse to the direct VPP effect regime with increasing surface tension. Overall, the exact results from our simulations reflect the same crossover behavior we revealed in Sec. II, from the one-loop perturbative results. This obser-

vation is striking, having in mind that the perturbation theory *a priori* cannot be directly applied to bare potentials with nonanalytic minima, as in Fig. 6. Moreover, somewhat surprisingly, we will show in the following that the similarity between the simulations data and one-loop results is *not* only qualitative. It will be argued on quantitative grounds that the simulations results can be very well quantitatively understood by assuming that the strongly entropic system (with nonanalytic intermanifold potentials, as in Fig. 6) can be described by analytic coarse-grained potentials, similar to the standard steric repulsion effective potential in Eq. (3.3).

In fact, our simulation results in Fig. 7 for 2D smectic stacks of semiflexible polymers ($d=1$) suggest some even more remarkable features.

(a) All the data can be fit, within a few percent accuracy, by using just one-loop formulas such as Eqs. (2.10) and (2.11). Applied to the reduced Hamiltonian of this section, Eq. (3.12) ($\overline{P'}=\overline{\kappa'}=1$), this means

$$\beta_N(n,d,\overline{\gamma'}) = \langle h'_{n+1}(\mathbf{x}') - h'_n(\mathbf{x}')\rangle = \beta_\infty(d) + A'_d[I_N(n,d,\overline{\gamma}) - I_\infty(d)] \quad (3.21)$$

and

$$\beta_N(d,\overline{\gamma'}) = \frac{\langle h'_N(\mathbf{x}') - h'_1(\mathbf{x}')\rangle}{N-1} = \beta_\infty(d) + A'_d[I_N(d,\overline{\gamma}) - I_\infty(d)], \quad (3.22)$$

with $\overline{\gamma'}$ and $\overline{\gamma}$ related by Eq. (3.15). This is documented in Figs. 7(b) and 7(a). There we fit *all* the data, obtained at six different values of the surface tension, by the one-loop equations (3.21) and (3.22), by treating the two parameters therein, $\beta_\infty(d)$ and A'_d, as fitting parameters. Surprisingly, these two-parameter fits provide an excellent description for all simulations data. Thus, Fig. 7(a) gives our simulations results for the constants $\beta_N(d,\overline{\gamma'})$ obtained from $6\times 9=54$ simulations, with different system sizes N and different surface tensions. Note that all 54 simulations could be fit remarkably well by just *two*-parameter one-loop fitting formula for $\beta_N(d,\overline{\gamma'})$ in Eq. (2.33), with $\beta_\infty(d=1)\cong 0.611$ and $A'_{d=1}\cong 0.161$. These values provide also the good fits to the simulations data for $\beta_N(n,d=1,\overline{\gamma'})$ in Fig. 7(b), by using the one-loop formula in Eq. (3.21).

(b) Another surprising finding is that these results for 2D sterically stabilized smectic phases of semiflexible polymers ($d=1$) can be rationalized simply by assuming that the appropriate coarse-grained potential to be used in the one-loop formulas (3.21) and (3.22) is *exactly the same* as the standard effective potential for the sterically stabilized smectic liquid crystals, Eq. (3.3). Indeed, by using Eq. (3.3) [with $k_BT=\kappa=1$, and $a_{min}=0$, as in the reduced rescaled Hamiltonian Eq. (3.12)], we find, using Eq. (2.18),

$$A'_d = \frac{2}{4+d}\left(\frac{4+d}{4-d}\right)^{d/4}\frac{S_d}{(2\pi)^d}\frac{1}{[\beta_\infty(d)]^{d/4}}. \quad (3.23)$$

For $d=1$ ($S_{d=1}=2$), with $\beta_\infty(d=1)\cong 0.611$, Eq. (3.23) indeed gives $A'_{d=1}\cong 0.161$, in a remarkable agreement with the aforementioned value of $A'_{d=1}$ fitting well all our Monte Carlo simulations in Fig. 7.

Let us summarize our quantitative findings on 2D smectic stack of semiflexible polymers ($d=1$) with purely hard-core repulsive [or with a binding potential as in Fig. 6(b), in the regime away from the unbinding transition]: The nonuniform interpolymer spacing $a_N(n,\gamma)$ and the average smectic period $a_N(\gamma)$ are exactly given, respectively, by Eqs. (3.18) and (3.19). The β-constants therein are given, to a very good approximation, by Eqs. (3.21) and (3.22), with $\beta_\infty(d=1)\cong 0.611$, and $A'_{d=1}\cong 0.161$, and $\overline{\gamma}$ therein given by $\overline{\gamma}=\sqrt{3\beta_\infty(d=1)/5}\cdot\overline{\gamma'}\cong 0.605\overline{\gamma'}$ [after Eq. (3.15)]. Here, the dimensionless surface tension $\overline{\gamma'}$ is related to the actual surface tension γ by Eq. (3.11).

We would like to note that this excellent agreement with the one-loop fitting formula was found by fitting the results of Monte Carlo simulations done in a moderate range of surface tensions (up to $\overline{\gamma'}=10$, as in Fig. 7). It should be stressed however that our one-loop fitting formula remains very good even for very large values of the surface tension γ, and for small systems with just $N=3$ semiflexible polymers (when one would normally suspect the use of a coarse-grained potential). Indeed, we are able to solve exactly the $N=3$ polymers stack model in the limit of infinite surface tension. The details are given in Appendix B, with the result

$$\beta_{N=3}(d=1,\gamma=\infty)\cong 0.416. \quad (3.24)$$

This is less than 5% smaller than the approximate value obtained by our one-loop formula Eq. (3.22), yielding $\beta_{N=3}(d=1,\gamma=\infty)\cong 0.438$. Figure 8(a) gives our one-loop formula results for $\beta_N(d=1,\gamma)$ versus N for $\gamma=0$ and ∞ [solid lines], as obtained by Eq. (3.22) with $\beta_\infty(d=1)\cong 0.611$ and $A'_{d=1}=0.161$.

Furthermore, in Fig. 8(b), we include also the corresponding results for 3D sterically stabilized smectic phases of membranes ($d=2$), by giving $\beta_N(d=2,\gamma)$ versus N for $\gamma=0$ and ∞ [solid lines], as obtained by Eq. (3.22) with $\beta_\infty(d=2)\cong 0.595$ and $A'_{d=2}\cong 0.190$. As detailed in Appendix B, we have obtained these values by relating the present constant osmotic pressure ensemble, in the limit $\gamma=\infty$, to the ensemble of membranes stacked between hard walls, that has been extensively studied over recent years [22,23]. As for $d=1$, for $d=2$ we also find that the one-loop formula Eq. (3.22) provides a very good fit to the existing data, both for $\gamma=\infty$ and for $\gamma=0$ [20]. For these two values of γ, Eq. (3.22), and Eqs. (2.21) and (2.22) provide nice closed formulas for the universal constants of membrane stacks

$$\beta_N(d=2,\gamma=0) = \beta_\infty(d=2) + A'_{d=2}\left\{\frac{\pi}{2(N-1)}\left[\cot\left(\frac{\pi}{4N}\right)-1\right]-2\right\} = \beta_\infty(d=2) + A'_{d=2}\frac{2-\frac{1}{2}\pi}{N}+\cdots \quad (3.25)$$

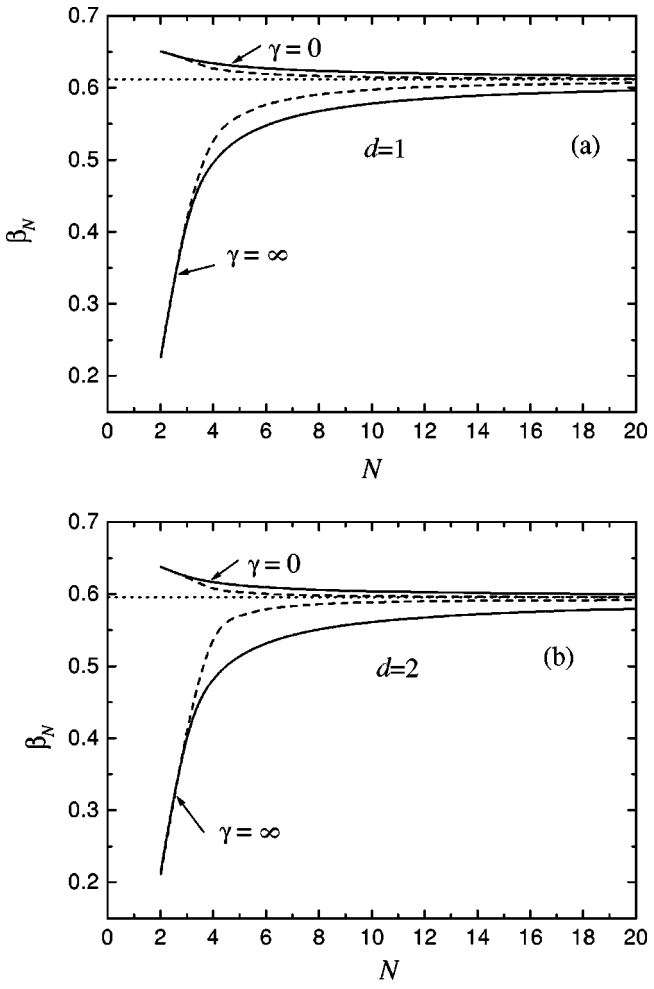

FIG. 8. Solid lines: $\beta_N(d,\gamma)$ for $\gamma=0$ and ∞, as the function of the number of manifolds N, obtained by $\beta_N(d,\gamma)=\beta_\infty(d)+A'_d[I_N(d,\gamma)-I_\infty(d)]$ for (a) N-polymer stack ($d=1$), and (b) N membrane stack ($d=2$). Dashed lines give $\beta_N(n_{mid},d,\gamma)=\beta_\infty(d)+A'_d[I_N(n_{mid},d,\gamma)-I_\infty(d)]$ versus N for $\gamma=0$ and ∞, for the layer in the middle of the stack with $n=n_{mid}=N/2$ for N even, and $n_{mid}=(N+1)/2$ for N odd. All the data are obtained by using $\beta_\infty(d=1)=0.611$ and $A'_{d=1}=0.161$, whereas $\beta_\infty(d=2)=0.595$ and $A'_{d=2}=0.190$.

and

$$\beta_N(d=2,\gamma=\infty)$$
$$=\beta_\infty(d=2)+A'_{d=2}\left\{\frac{\pi}{2(N-1)}\left[\cot\left(\frac{\pi}{4(N-1)}\right)-1\right]-2\right\}$$
$$=\beta_\infty(d=2)-A'_{d=2}\frac{\frac{1}{2}\pi}{N}+\cdots \tag{3.26}$$

depicted in Fig. 8(b). The limits $\gamma=0$ and $\gamma=\infty$ play special role in the applications of our theory to the realistic system, as detailed in Sec. IV. In contrast to the $d=1$ case, for membranes ($d=2$), the value $A'_{d=2}\cong 0.190$ obtained by fitting to the data is substantially different from the value that would be suggested by Eq. (3.23) (yielding $A'_{d=2}=0.119$). This difference simply indicates that the appropriate coarse-grained potential is not exactly the same as the standard effective potential Eq. (3.3). We note that these two potentials need not be identical. Their near coincidence that we found for 2D sterically stabilized smectic stacks of semiflexible polymers ($d=1$) is thus a puzzling but not essential feature of our discussions here.

Overall, the one-loop theory results provide quantitatively very good description of finite-size effects in sterically stabilized smectic stacks of both semiflexible polymers and membranes. With this in mind, using Eqs. (3.20) and (3.22), we have, for the smectic period $a_N(\gamma)$,

$$a_N(\gamma)-a_\infty=\frac{A'_d}{\beta_\infty(d)}[I_N(d,\overline{\gamma})-I_\infty(d)](a_\infty-a_{min}), \tag{3.27}$$

with $\overline{\gamma}=\overline{\gamma}'\sqrt{(4-d)\beta_\infty(d)/(4+d)}$; here $\overline{\gamma}'=\gamma(k_BT)^{2/(4+d)}/\kappa^{(2+d)/(4+d)}P^{4/(4+d)}$, see Eqs. (3.11) and (3.15). As in Sec. II, the finite-size effect expressed by Eq. (3.27) decays as $1/N$, reflecting the general exact result stated in Eq. (2.40). From Eqs. (3.27) and (2.41), we find, for $N\gg 1$,

$$a_N(\gamma)-a_\infty\approx\frac{\lambda(\gamma)}{N} \tag{3.28}$$

with

$$\lambda(\gamma)=\frac{A'_dC_1(d,\overline{\gamma})}{\beta_\infty(d)}(a_\infty-a_{min}), \tag{3.29}$$

to be compared with similar results in Sec. II [see Eqs. (2.42) and (2.43)]. Let us consider these results for the stacks of membranes ($d=2$). With the aforementioned values of $A'_{d=2}$ and $\beta_\infty(d=2)$, we have $[A'_d/\beta_\infty(d)]_{d=2}\cong 0.319$, whereas $C_1(\overline{\gamma},d)$ is in the range between $C_1=2-\pi/2$ for $\gamma=0$ and $C_1=-\pi/2$ for $\gamma=\infty$. Thus, from Eq. (3.29), $\lambda(\gamma)$ is in the range between $\lambda(\gamma=0)$ and $\lambda(\gamma=\infty)$, with

$$\lambda(\gamma=0)=+0.137(a_\infty-a_{min}) \tag{3.30}$$

and

$$\lambda(\gamma=\infty)=-0.502(a_\infty-a_{min}). \tag{3.31}$$

Equations (3.28)–(3.31) provide useful estimates of the magnitude of finite-size effects for $N\gg 1$. More generally, for a finite but not necessarily large N, for membranes stacks we have, by using Eq. (3.27), with $[A'_d/\beta_\infty(d)]_{d=2}\cong 0.319$, and Eqs. (2.21) (for $\gamma=0$) and (2.22) (for $\gamma=\infty$),

$$a_N(\gamma=0)-a_\infty$$
$$=0.319\left\{\frac{\pi}{2(N-1)}\left[\cot\left(\frac{\pi}{4N}\right)-1\right]-2\right\}(a_\infty-a_{min}) \tag{3.32}$$

and

$$a_N(\gamma=\infty)-a_\infty = 0.319\left\{\frac{\pi}{2(N-1)}\left[\cot\left(\frac{\pi}{4(N-1)}\right)-1\right]-2\right\}(a_\infty-a_{min}). \tag{3.33}$$

Let us now address the magnitude of these effects, in relation to our previous discussion of the experiments of Katsaras [17] aimed to investigate the VPP phenomenon (see Sec. I, and the end of Sec. II). As noted before in this section, at room temperature the actual experimental membrane system may be characterized as a strongly entropic system with bare binding potential with a sharp minimum, of the form depicted in Fig. 6(b). Away from membrane unbinding transition, the physics going with this potential is the same as in the sterically stabilized phases under an osmotic pressure (recall the discussion of Fig. 6). We can thus use the above results to argue about the visibility of VPP effects in the experimental system of Katsaras with the bound stacks of DMPC membranes [17]. For these systems, experimentally the stack period $a_\infty \approx 6.2$ nm, whereas a_{min} can be identified with the position of the minimum of potential (2.45), $a_{min} \cong r_0 \approx 5.64$ nm, by the results of Sec. II. Thus, the thermal stack period expansion $a_\infty - a_{min} \cong a_\infty - r_0 \approx 0.56$ nm. For example, let us consider the limit $\gamma=\infty$, where the VPP effect is the strongest. From Eqs. (3.31) and (3.28), $a_N - a_\infty \approx -0.501\times 0.56$ nm$/N \approx -0.28$ nm$/N$. Thus, with N in the range between $N=600$ and 1800 membranes, as in the experiments of Katsaras [17], $a_N - a_\infty$ is in the range between -4.6×10^{-4} nm and -1.6×10^{-4} nm. So, the magnitude of the finite-size effect, $a_N - a_\infty$, is hundred times smaller than 3×10^{-2} nm, which is the maximum accuracy in the experiments of Katsaras [17]. Thus, our results well explain the absence of a noticeable VPP effect in these experiments. By requiring that $|a_N - a_\infty|$ be within the experimental accuracy, one has 0.28 nm$/N > 3\times10^{-2}$ nm, yielding $N<9$ membranes. Thus, for $N>10$ membranes, the VPP effect becomes practically unobservable in these experiments. Recall that we have reached quantitatively the same conclusion in our discussions in Sec. II, through the application of the one-loop theory to the bare interaction potential (2.45), which is marginally strongly entropic at room temperature. It has been pointed out however that the results obtained in that way may be unwarranted (at room temperature). It is thus pleasing to see that the more careful treatment of strong entropic effects, presented in this section, yields nearly the same quantitative estimates. It should be stressed that this is not a result of a simple coincidence, but rather a consequence of the fact that a strongly entropic system can be quantitatively well treated by the one-loop theory in combination with suitably defined effective potentials. Due to this, we had a strong similarity of the results presented in this section with the results of Sec. II. Thus, Eq. (3.27) of this section can be given in the form

$$a_N(\gamma)-a_\infty = Q(d)\left[\frac{I_N(d,\overline{\gamma})}{I_\infty(d)}-1\right](a_\infty-a_{min}) \tag{3.34}$$

with $Q(d)=A'_d I_\infty(d)/\beta_\infty(d) = A'_d B(1-d/4,d/2)/\beta_\infty(d)$. Up to the proportionality constant $Q(d)$, Eq. (3.34) is remarkably the same as Eq. (2.44) of Sec. II. Finally, it is interesting to note that, surprisingly, the constant $Q(d)$ has nearly the same value for $d=1$ and $d=2$. Indeed, for $d=1$, by using our fit values $A'_{d=1}=0.161$, $\beta_\infty(d=1)=0.611$, and $B(3/4,1/2)=2.3963$, we find $Q(d=1)\cong 0.631$. Likewise, for $d=2$, by using the aforementioned values $A'_{d=2}=0.190$, $\beta_\infty(d=2)=0.595$, and $B(1/2,1)=2$, we find $Q(d=2)\cong 0.639$. Thus, to a high, 1% accuracy, $Q(d=1)\cong Q(d=2)$. Understanding this (at least approximate) superuniversality of $Q(d)$ is beyond our scope here. We point it however as an inspiration for future studies. Another (likely related) aspect left for future studies is to explain the high accuracy provided by the simple one-loop formulas in fitting the results from Monte Carlo simulations. How come that we did not need, say, two-loop contribution to fit all the results with a high (few percent) accuracy?

Finally, let us elucidate the behavior of the local smectic (intermanifold) interlayer distances, $a_N(n)=\langle h_{n+1}(\mathbf{x}) - h_n(\mathbf{x})\rangle$, for the nth layer of an N-manifold stack. For them we have, from Eqs. (3.2), (3.18) and (3.21),

$$a_N(n,\gamma)-a_\infty = \left[\frac{\beta_N(n,d,\overline{\gamma'})}{\beta_\infty(d)}-1\right](a_\infty-a_{min}) = Q(d)\left[\frac{I_N(n,d,\overline{\gamma})}{I_\infty(d)}-1\right](a_\infty-a_{min}). \tag{3.35}$$

In Fig. 9, we plot the ratio $I_N(n,d,\overline{\gamma})/I_\infty(d)$ for the interesting limits $\gamma=0$ and $\gamma=\infty$, for $d=1$ and $d=2$, for stacks of various sizes N. It is instructive to compare the local interlayer distances in Eq. (3.35) with their stack average value $a_N(\gamma)$, see Eqs. (3.20) and (3.34). From Eq. (3.35) and Fig. 9, we see that, for stacks with $N>10$ manifolds, highly nonuniform interlayer distances occur only close to the stack surfaces. The interlayer distances close to stack center, $a_N(n_{mid})$ with $n_{mid}\approx N/2$, approach their thermodynamic limit more quickly than the average stack period a_N. This is evidenced in Fig. 8, depicting β_N (solid lines) for the whole stack period [see Eq. (3.20)], and $\beta_N(n_{mid})$ (dashed lines) for the interlayer distances at the stack center [see Eq. (3.35)]. Obviously, $\beta_N(n_{mid})$ approaches its thermodynamic limit β_∞ more quickly than β_N. Thus, importantly, $|a_N(n_{mid},\gamma)-a_\infty| \ll |a_N-a_\infty|$ for $N\gg 1$. In fact, recall that $a_N-a_\infty \sim 1/N$, whereas, from Eq. (3.35), $|a_N(n_{mid})-a_\infty| \sim 1/N^{1+d/2}$, as already noted in Sec. II. It follows that the main contribution to the difference a_N-a_∞ comes from the layers close to the stack interfaces rather than those close to its center. Figure 9 clearly documents this feature [see also Sec. II, Eqs. (2.38)–(2.41), and discussions therein]. Experimental implications of this fact are discussed in Sec. IV [see item (4) therein].

IV. COMMENTS AND SUMMARY

We begin this section by commenting on the effects of a typically large value of water liquid-vapor surface tension γ. It will be convenient to express γ as

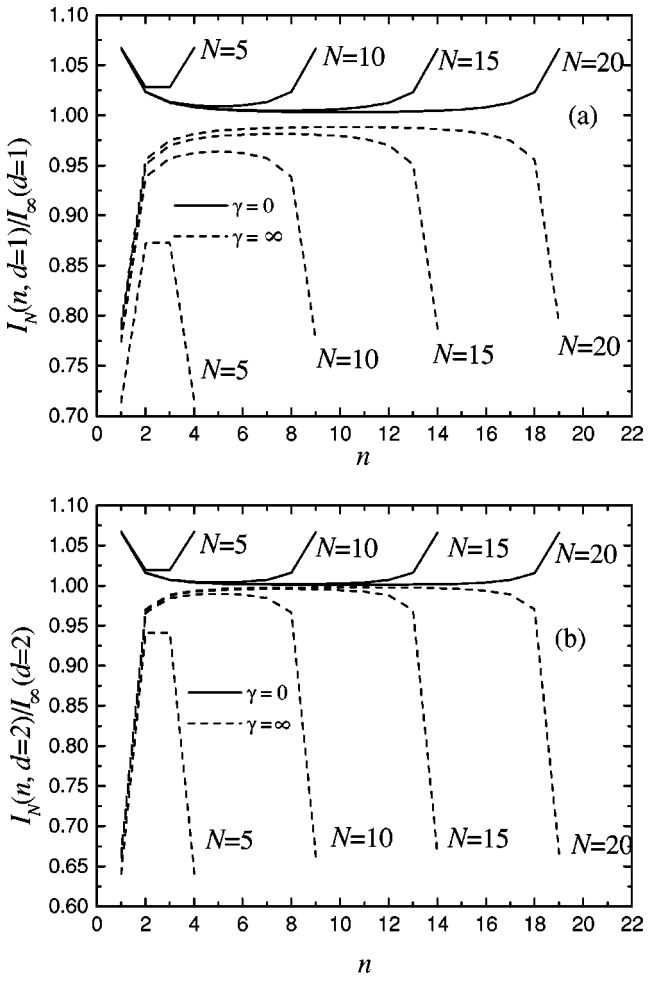

FIG. 9. The universal functions $I_N(n,d,\bar{\gamma})/I_\infty(d)$ for $\gamma=0$ (solid lines) and $\gamma=\infty$ (dashed lines), for (a) various 2D stacks of N semiflexible polymers, $d=1$, and (b) various 3D stacks of N fluid membranes, $d=2$. We note that for $d=2$, $I_\infty(d=2)=2$, whereas $I_N(n,d,\bar{\gamma})$ for $\gamma=0$ and $\gamma=\infty$ is given analytically by Eqs. (2.23) and (2.24).

$$\gamma=\frac{k_BT}{l_\gamma^2}. \tag{4.1}$$

Here, $l_\gamma=\sqrt{k_BT/\gamma}$ is a characteristic surface tension length scale. Typically, l_γ is small compared to the lamellar phase period a. Indeed, with $\gamma\approx 70\times 10^{-3}$ J/m^2, one has $l_\gamma \approx 0.24$ nm at room temperature, whereas $a\sim 6$ nm, for bound stacks of membranes [see Sec. II end], or even $a \sim 50$ nm for highly swollen phases of unbound membranes [2,10–12]. The large separation between the length scale l_γ and the stack period a has profound implications on the magnitude of dimensionless surface tension $\bar{\gamma}=\gamma/\delta\gamma$, introduced in Sec. II, see Eqs. (2.13) and (2.14). For example, for sterically stabilized membrane phases, $\delta\gamma=\sqrt{\kappa b_2}$, with $b_2 = -\partial P/\partial a = +\partial^2 V_{eff}/\partial a^2$. Here V_{eff} is as in Eq. (3.3), with $d=2$, yielding

$$b_2=3\alpha_\infty(d=2)\frac{(k_BT)^2}{\kappa l^4}=3\frac{P}{l} \tag{4.2}$$

and

$$\delta\gamma=\sqrt{3\alpha_\infty(d=2)}\,\frac{k_BT}{l^2}, \tag{4.3}$$

with $\alpha_\infty(d=2)=[\beta_\infty(d=2)]^3\cong 0.212$ (see Sec. III), and $l=a-a_{min}$, membrane surface-to-surface separation (a_{min}, the membrane thickness). Using Eqs. (4.2) and (4.3), the dimensionless surface tension

$$\bar{\gamma}=\frac{\gamma}{\delta\gamma}=\frac{1}{\sqrt{3\alpha_\infty(d=2)}}\left(\frac{l}{l_\gamma}\right)^2\cong 1.25\left(\frac{l}{l_\gamma}\right)^2. \tag{4.4}$$

For, say, $l\approx 1$ nm and $l_\gamma\approx 0.24$ nm, from Eq. (4.4), we have $\bar{\gamma}\approx 20$. So, $\bar{\gamma}\gg 1$ for the sterically stabilized system of repelling membranes, even for the modest membrane separations. Essentially, the same estimate as in Eq. (4.3) is obtained also for the bound stacks of membranes, for the realistic situations with strong entropic effects [see Sec. III, the discussion of Fig. 6(b) therein]. Thus, quite generally for strongly entropic systems, $\bar{\gamma}\gg\bar{\gamma}^*(d=2)\cong 0.592$ [see Sec. II and Fig. 5(b)]. It would be thus tempting to assume that, to a good approximation, one can apply to these systems the results of Secs. II and III in the limit $\bar{\gamma}\to\infty$ [see, e.g., Eqs. (2.22), (2.29), (3.31), and (3.33), and Fig. 7]. This conclusion is however unwarranted as the liquid-vapor interface is not firmly bound to the outmost membranes of the stack, as assumed in the discussion of Secs. II and III. Elsewhere, in Ref. [29], we reexamine our results in light of a more realistic model that incorporates the degrees of freedom associated with liquid-vapor interfaces. Interactions between these interfaces and nearby membranes are typically repulsive, and liquid-vapor interfaces are generally expected to unbind from the stack for $P\to 0$. This may provide a mechanism weakening the surface tension VPP effects, as already noted by Nagle and Katsaras [18]. In Ref. [29] we find that this is indeed the case for the *bound* stacks of manifolds such as DMPC bilayers discussed in Secs. II and III. For such stacks, in the limit of zero surface osmotic pressure, $P\to 0$, the stack period a_N approaches a finite value, whereas the vapor-liquid interface completely unbinds from the stack under the influence of repulsive (disjoining) van der Waals forces, as we detail in Ref. [29]. For $P\to 0$, such stacks behave exactly as the zero surface tension stacks in Secs. II and III [see also Fig. 1(e), and the discussion following Eq. (2.4)]. Thus, for example, using Eq. (3.32) [or Eq. (3.34) with $\bar{\gamma}=0$], for the average period of N-membrane stacks we have

$$a_N=\frac{\langle h_N(\mathbf{x})-h_1(\mathbf{x})\rangle}{N-1}$$
$$=a_\infty+Q(d=2)\left\{\frac{\pi}{4(N-1)}\left[\cot\left(\frac{\pi}{4N}\right)-1\right]-1\right\}(a_\infty-r_0) \tag{4.5}$$

with $Q(d=2)\cong 0.639$, and, for example, $a_\infty-r_0\approx 0.56$ nm being the thermal expansion for DMPC [see Sec. III]. Likewise, the local average intermembrane spacings are given by

$$a_N(n)=\langle h_{n+1}(\mathbf{x})-h_n(\mathbf{x})\rangle = a_\infty+Q(d=2)\left[\frac{I_N(n,d=2,\bar{\gamma}=0)}{2}-1\right](a_\infty-r_0), \tag{4.6}$$

with $I_N(n,d=2,\bar{\gamma}=0)$ explicitly given by Eq. (2.23). We note that for practically significant limit $N\gg 1$, from Eq. (4.5), we have also the equation

$$a_N-a_\infty\cong\frac{1}{2}\left(2-\frac{\pi}{2}\right)Q(d=2)\,\frac{a_\infty-r_0}{N}\cong 0.137\frac{a_\infty-r_0}{N}, \tag{4.7}$$

providing a useful simple result for discussing the experimental visibility of finite-size effects in the bound stacks at zero osmotic pressure, as exemplified for the case of DMPC in Sec. III. We note that here $a_N>a_\infty$ in Eqs. (4.5) and (4.7) reflecting the presence of our reverse VPP effect [Fig. 1(c)] revealed in Secs. II and III.

A different behavior is found for the *unbound*, sterically stabilized stacks of membranes. For them, too, for $P\to 0$, the tense vapor-liquid interfaces unbind from the stack, due to repulsive van der Waals forces [29]. However, for $P\to 0$, the tensionless stack membranes themselves also unbind. Intermembrane separation diverges *faster* than the separation between the stack and the vapor-liquid interfaces, as we detail in Ref. [29]. There, we show that from $P\to 0$, i.e., for highly swollen stacks we can directly use our results of Sec. III obtained in the limit of infinite surface tension. Thus, for example, using Eq. (3.33) [or Eq. (3.34)], for the average period of N-membrane stacks we have

$$a_N=\frac{\langle h_N(\mathbf{x})-h_1(\mathbf{x})\rangle}{N-1} = a_\infty+Q(d=2)\left\{\frac{\pi}{4(N-1)}\left[\cot\left(\frac{\pi}{4(N-1)}\right)-1\right]-1\right\}\times(a_\infty-a_{min}) \tag{4.8}$$

with $Q(d=2)\cong 0.639$, and $a_\infty-a_{min}=\beta_\infty(d=2)\times(k_BT)^{2/3}/\kappa^{1/3}P^{1/3}$, with $\beta_\infty(d=2)=0.595$ (see Sec. II). Likewise, the local average intermembrane spacings are given by

$$a_N(n)=\langle h_{n+1}(\mathbf{x})-h_n(\mathbf{x})\rangle = a_\infty+Q(d=2)\left[\frac{I_N(n,d=2,\bar{\gamma}=\infty)}{2}-1\right](a_\infty-a_{min}) \tag{4.9}$$

with $I_N(n,d=2,\bar{\gamma}=\infty)$ explicitly given by Eq. (2.24). We note that, for the practically significant limit $N\gg 1$, using Eq. (4.8), we have also the equation

$$a_N-a_\infty\cong-\frac{\pi}{4}Q(d=2)\frac{a_\infty-a_{min}}{N}\cong-0.502\frac{a_\infty-a_{min}}{N}, \tag{4.10}$$

providing a useful simple result for discussing the experimental visibility of VPP effects in these systems. We note that here $a_N<a_\infty$ in Eqs. (4.8) and (4.10) reflecting the presence of the ordinary VPP effect [Fig. 1(b)], as detailed in Secs. II and III.

Let us summarize our major results and compare them with the previous theoretical study of Podgornik and Parsegian, Ref. [14].

(1) We find that both the reverse ($a_N>a_\infty$) and ordinary ($a_N<a_\infty$) finite-size VPP effects may be present in smectic stacks of N semiflexible manifolds, as conceptualized in Fig. 1. The magnitude of these effects is limited by the magnitude of the stack thermal expansion. For example, for $N\gg 1$, we find that $a_N-a_\infty\cong\lambda/N$, with $|\lambda|\sim|a_\infty-r_0|$ being the stack period thermal expansion away from $T=0$ smectic period r_0. As detailed in Secs. II and III, this feature of our theory well explains the absence of noticeable VPP effects in the experiments of Katsaras [17]. $\lambda(\gamma)$ depends on the surface tension of interfacial manifolds. However, it has finite limits for $\gamma\to 0$ and $\gamma\to\infty$. For example, $\lambda(0)=-0.137(a_\infty-r_0)$, $\lambda(\infty)=+0.502(a_\infty-r_0)$, for entropically dominated membrane stacks [in both unbound and bound lamellar phases, see Sec. III]. This result is in contrast to the corresponding results of Podgornik and Parsegian in Ref. [14], yielding much larger λ, for example, $\lambda(\infty)=-(1/3\alpha_\infty)\times[(a_\infty-r_0)/\Delta x]^2(\kappa/k_BT)(a_\infty-r_0)$. In their theory, $|\lambda|\gg|a_\infty-r_0|$, as $\kappa/k_BT\sim 10$, and, more importantly, $|a_\infty-r_0|\gg\Delta x$ is the short-distance cutoff [$\Delta x\sim 1$ nm, the lipid molecule size]. Note that for the unbound stacks of membranes with $a_\infty-r_0\approx a_\infty\sim 100$ nm$\gg\Delta x$, the Podgornik-Parsegian result for $\lambda(\infty)$ exceeds the thermal stack period expansion by a factor of 10^4. Moreover, the Podgornik-Parsegian theory strangely predicts that the smectic period a_N of sterically stabilized (purely repelling) membrane stack approaches a *finite* value $(a_N)_{max}=a_{min}+(\alpha k_BT/\kappa)^{1/2}\Delta x\sqrt{N}$, in the limit of zero osmotic pressure, $P\to 0$. Such an unexpected effect has never been observed in a sterically stabilized system of unbound membranes, and contradicts any common intuition on the behavior of purely repelling manifolds. Our theory is free of such unphysical results. See, for example, our Eqs. (3.2), (3.9), (3.16), (3.33), (4.7), or (4.10), all manifestly showing that $a_N\sim 1/P^{1/3}\to\infty$ as $P\to 0$. We stress, this is an exact (nonperturbative) result.

(2) So, what is causing the problems in the theory of Podgornik and Parsegian? It is the very first assumption done in the theory, to use the smectic continuum elastic model, the standard Landau-Peierls model of smectic liquid crystals, which ignores the layered character of the smectic liquid crystals and replaces the smectic displacement $u_n(\mathbf{x})$ with the continuum field $u(z,\mathbf{x})$, with $z=na$. Next, it was assumed that the smectic z coordinate is essentially continuous ($\Delta z=0$), whereas the only short-distance cutoff is Δx (lipid molecule size). However, truly $\Delta z=a$ (smectic phase period) and, in practical situations, $\Delta z>\Delta x$. So, taking $\Delta z=0$ and keeping Δx as the only short-distance cutoff is obviously a problematic assumption of the theory of Podgornik and Parsegian. It is the major cause of the difficulties of their theory discussed in item (1) above. This assumption yields large and

unphysical predictions for the VPP phenomena in Ref. [14]. These problems culminate in their prediction of the artificial maximum period $(a_N)_{max} \sim \Delta x \sqrt{N}$ for the sterically stabilized lamellar phases of purely repelling membranes [note that, strangely, this $(a_N)_{max}$ goes to zero for $\Delta x \to 0$].

(3) In contrast to the theory of Podgornik and Parsegian, our theory does not make the assumption that the smectic z coordinate is continuous. Rather than using the continuous Landau-Peierls model, we keep in our calculations the discrete, layered character of smectic liquid crystals, by describing smectic layers by their height functions $h_n(\mathbf{x})$, $n = 1,2,3,\ldots,N$. Thus, rather than dealing with the smectic continuum model employed by Podgornik and Parsegian, we employ here a more microscopic smectic model with N interacting semiflexible manifolds. Within this approach, importantly, all interesting results [smectic average period, etc.] have a finite value in the continuum limit $\Delta x \to 0$, in contrast to the results of Podgornik and Parsegian in Ref. [14]. In fact, throughout this paper we presented our results in the limit $\Delta x \to 0$ (corrections due to a nonzero Δx are small in practical situations, see the end of Appendix A).

(4) An essential feature of our results here is the spatially nonuniform character of smectic interlayer distances, $a_N(n) = \langle h_{n+1}(\mathbf{x}) - h_n(\mathbf{x}) \rangle$, for the nth layer of an N-manifold stack. They have not been calculated in the previous studies of the VPP phenomena. Thus, the Podgornik-Parsegian theory, Ref. [14], effectively assumes that interlayer distances are uniform, n-independent, and schematically describes VPP effects in terms of pseudo-Casimir forces. We have demonstrated here that such a picture obscures the real nature of the VPP phenomena. Their essence is in spatially nonuniform thermal expansion of smectic interlayer distances as revealed in Sec. II [see the discussion following Eq. (2.34)]. We have found that the VPP phenomenon itself, i.e., the difference $a_N - a_\infty$, is in large part related to the behavior of local interlayer distances $a_N(n)$ in the regions close to the stack interfaces, see Eqs. (2.38)–(2.41), and the discussions at the end of Sec. III, and Figs. 8 and 9 therein. Here, we recall that $a_N - a_\infty \sim 1/N$, whereas for the interlayer distances $a_N(n)$ close to the stack center, $n \approx N/2$, we have $a_N(n = N/2) - a_\infty \sim 1/N^{1+d/2} \ll 1/N$. Thus, we have $|a_N(n = N/2) - a_\infty| \ll |a_N - a_\infty|$, and the main contribution to the difference between the stack average period a_N and its thermodynamic limit value a_∞ comes from the layers close the stack surfaces, as evidenced in Fig. 9. This fact provides further severe limitations to the experimental observations of VPP phenomena based on standard x-ray diffraction (Fourier transform) techniques which are probing interlayer distances close to the center of the stack. For them we have $a_N(n = N/2) - a_\infty \approx (a_N - a_\infty)/N^{d/2}$. Thus, for membrane stack ($d = 2$), with $N \sim 1000$ (as in the experiments of Katsaras [17]), $a_N(n = N/2) - a_\infty$ is about thousand times smaller than $a_N - a_\infty$, which itself is already smaller than the experimental resolution [see Secs. II and III]. As detailed in Secs. II and III, finite-size VPP effects are practically significant only in small stacks with up to $N \sim 10$ manifolds such as the thin smectic film [26].

(5) Beyond the significance for VPP effects, our results are of a more fundamental interest for the statistical mechanics investigations of smectic stacks, such as the work of Bachmann *et al.* [22]. We find that finite-size effects in strongly entropic stacks, such as the sterically stabilized phases, can be described *quantitatively* well by a simple analytic one-loop theory [see Sec. III]. The assumption underlying the success of such an approach to these nonperturbative problems, namely, the existence of suitably defined effective (coarse-grained) potentials is well documented by the present study, by carefully relating the analytic theory of Sec. II to Monte Carlo simulations of Sec. III. We highlight this finding because of its interest for future theoretical studies of smectic stacks of manifolds.

ACKNOWLEDGMENTS

We thank Rudi Podgornik for bringing the VPP phenomena to our attention. These contacts have been, in part, aided by the kind hospitality of the Aspen Center for Physics.

APPENDIX A:

Here, we discuss the results outlined in Sec. II. First, we present the derivation of our Eq. (2.7). Prior to giving its formal derivation, we give a simple physical interpretation of the one-loop perturbation theory result for local smectic spacings in Eq. (2.7). The result is easily rationalized by considering the interaction part of the smectic Hamiltonian of Sec. II,

$$H_{int} = \int d^d\mathbf{x} \left\{ \sum_{n=1}^{N-1} V_{net}(h_{n+1}(\mathbf{x}) - h_n(\mathbf{x})) \right\} = \int d^d\mathbf{x} \left\{ \sum_{n=1}^{N-1} \left[b_0 + \frac{b_2}{2}[e_n(\mathbf{x})]^2 + \frac{b_3}{3!}[e_n(\mathbf{x})]^3 + \cdots \right] \right\} \tag{A1}$$

with $e_n(\mathbf{x}) = u_{n+1}(\mathbf{x}) - u_n(\mathbf{x}) = h_{n+1}(\mathbf{x}) - h_n(\mathbf{x}) - r_0$. Within the harmonic approximation ($b_3 \to 0$, etc.), one has $\langle e_n(\mathbf{x}) \rangle = 0$, i.e., $\langle h_{n+1}(\mathbf{x}) - h_n(\mathbf{x}) \rangle_0 = r_0$, simply because the harmonic smectic Hamiltonian has the symmetry $e_n(\mathbf{x}) \to -e_n(\mathbf{x})$. This symmetry is however broken by the odd anharmonic terms such as $b_3[e_n(\mathbf{x})]^3/3!$, etc. Thus, $\langle e_n(\mathbf{x}) \rangle \neq 0$, in general, due to the anharmonic terms. A simple and appealing way to see this is by replacing in Eq. (A1) the cubic term $b_3 e_n(\mathbf{x}) e_n(\mathbf{x}) e_n(\mathbf{x})/3!$ by the term $C e_n(\mathbf{x}) \langle [e_n(\mathbf{x})]^2 \rangle_0 / 3!$, with C being a numerical constant. This self-consistent "statistical linearization" of the problem can be shown to yield the correct result (to one-loop order) provided $C = 3$, see below. With this self-consistent approximation,

$$H_{int} = \int d^d\mathbf{x} \left\{ \sum_{n=1}^{N-1} \left[b_0 + \frac{b_2}{2}[e_n(\mathbf{x})]^2 + C\frac{b_3}{3!}\langle [e_n(\mathbf{x})]^2 \rangle_0 e_n(\mathbf{x}) \right] \right\}. \tag{A2}$$

Thus, the cubic term produces an effective entropic local stress $\sim b_3 \langle [e_n(\mathbf{x})]^2 \rangle_0$ in the second term of Eq. (A2). This

stress introduces a nonzero local strain $\langle e_n(\mathbf{x})\rangle$, which can be simply obtained by minimizing the above H_{int} in Eq. (A2) over $e_n(\mathbf{x})$. This easily yields

$$\langle h_{n+1}(\mathbf{x})-h_n(\mathbf{x})\rangle - r_0 \equiv \langle e_n(\mathbf{x})\rangle = -\frac{Cb_3}{3!b_2}\langle [e_n(\mathbf{x})]^2\rangle_0 = -\frac{Cb_3}{3!b_2}\langle [u_{n+1}(\mathbf{x})-u_n(\mathbf{x})]^2\rangle_0 . \tag{A3}$$

Equation (A3), with $C=3$, is indeed in accord with Eq. (2.7). Equation (A3) is strictly valid as the leading (one-loop) term of the low-temperature expansion. Indeed, in the low-T limit, it suffices to keep only the cubic anharmonic term

$$H_{int}^{(3)} = \sum_{n=1}^{N-1} \int d^d\mathbf{x} \frac{b_3}{3!}[e_n(\mathbf{x})]^3 \tag{A4}$$

in Eq. (A1). By expanding the Boltzmann factor in powers of this term, one has the perturbation expansion,

$$\langle e_n(\mathbf{x})\rangle = \langle e_n(\mathbf{x})\rangle_0 - \frac{1}{k_BT}[\langle e_n(\mathbf{x})H_{int}^{(3)}\rangle_0 - \langle e_n(\mathbf{x})\rangle_0\langle H_{int}^{(3)}\rangle_0 + \cdots], \tag{A5}$$

where, as before, $\langle\cdots\rangle_0$ signifies the average with respect to the harmonic stack Hamiltonian Eq. (2.9) [or, Eq. (A9) below]. As $\langle e_n(\mathbf{x})\rangle_0 = 0$, we thus have

$$\langle e_n(\mathbf{x})\rangle = -\frac{1}{k_BT}\langle e_n(\mathbf{x})H_{int}^{(3)}\rangle_0 \tag{A6}$$

to the leading order at low T. For the harmonic average on the right-hand side of this equation, we have, by the Wick theorem,

$$\langle e_n(\mathbf{x})\rangle = -\frac{1}{k_BT}\frac{b_3}{3!}\left\langle e_n(\mathbf{x})\sum_{n'=1}^{N-1}\int d^d\mathbf{x}'[e_{n'}(\mathbf{x}')]^3\right\rangle_0 = -\frac{1}{k_BT}\frac{3b_3}{3!}\sum_{n'=1}^{N-1}\int d^d\mathbf{x}'\langle e_n(\mathbf{x})e_{n'}(\mathbf{x}')\rangle_0 \times\langle [e_{n'}(\mathbf{x}')]^2\rangle_0 . \tag{A7}$$

For a harmonic smectic Hamiltonian with just nearest neighbor interactions (such as Eq. (2.9), or Eq. (A9) below), it is straightforward to show that

$$\int d^d\mathbf{x}'\langle e_n(\mathbf{x})e_{n'}(\mathbf{x}')\rangle_0 = \langle e_n(\mathbf{q})e_{n'}(-\mathbf{q})\rangle_0|_{q=0} = \frac{\delta_{nn'}k_BT}{b_2}. \tag{A8}$$

By noting that $\langle [e_{n'}(\mathbf{x}')]^2\rangle_0$ on the right-hand side of Eq. (A7) does not depend on $\mathbf{x}'$, and by using Eq. (A8), we find that Eq. (A7) yields Eq. (A3) with $C=3$, i.e., Eq. (2.7).

Next, we outline here the derivation of Eqs. (2.10)–(2.15) by calculating the harmonic average in Eq. (2.7), i.e., Eq. (A3). For a general value of the surface tension γ, such calculation poses a difficult but tractable analytic problem, see Refs. [12] and [26]. Here, we will solve this problem by the method of effective Hamiltonians elaborated in our recent study [12]. To obtain the average in Eq. (2.7), we consider the harmonic smectic Hamiltonian Eq. (2.9) in the form

$$H_0 = \int_q \left[\sum_{n=2}^{N-1}\frac{1}{2}\kappa q^4|\tilde{u}_n(\mathbf{q})|^2 + \sum_{n=1}^{N-1}\frac{b_2}{2}|\tilde{u}_{n+1}(\mathbf{q})-\tilde{u}_n(\mathbf{q})|^2 + K_{surf}^{(1)}(q)|\tilde{u}_1(\mathbf{q})|^2 + K_{surf}^{(N)}(q)|\tilde{u}_N(\mathbf{q})|^2\right], \tag{A9}$$

with $\int_q = \int d^dq/(2\pi)^d$ and $\tilde{u}_n(\mathbf{q})$ being the Fourier transform of $u_n(\mathbf{x})$. The average in Eq. (2.7) involves only $u_{n+1}(\mathbf{x})$ and $u_n(\mathbf{x})$. This harmonic average can be found exactly by constructing an effective Hamiltonian for $u_{n+1}(\mathbf{x})$ and $u_n(\mathbf{x})$, $H_{eff}(u_{n+1},u_n)$, that is obtained by minimizing H_0 in Eq. (A9) for a fixed shape of the manifolds $u_n(\mathbf{x})$ and $u_{n+1}(\mathbf{x})$. First, let us consider the manifolds under the nth manifold and obtain the effective Hamiltonian $H_{eff}(u_n)$ for the nth manifold by minimizing H_0 Eq. (A9) over $u_1,u_2,\ldots,u_{n-1}$ for a fixed u_n. This minimization can be done in several interesting ways. For example, as detailed in Ref. [12], such a problem can be reduced (by successive minimizations over $u_1,u_2,\ldots,u_{n-1}$) to iterating the recursion relation

$$K_{m+1}(q) = \kappa q^4 + \frac{b_2K_m(q)}{b_2+K_m(q)}, \quad m=1,2,3,\ldots,n-1 \tag{A10}$$

with the initial condition

$$K_1(q) = K_{surf}^{(1)}(q). \tag{A11}$$

After $(n-1)$ iteration steps, all the manifolds except the last one, u_n, are integrated out, and one regains the effective Hamiltonian

$$H_{eff}(u_n) = \int_q \frac{1}{2}K_n(q)|\tilde{u}_n(q)|^2. \tag{A12}$$

Our task now is to find the dispersion relation $K_n(q)$ by iterating Eq. (A10). For this purpose, it is interesting to note that the recursion relation Eq. (A10) can be mapped into the calculation of the *equivalent resistance* of the circuit shown in Fig. 10(a) with resistances $K_m(q)$, κq^4, and b_2. Consequently, $K_n(q)$ is the equivalent resistance of the ladder circuit in Fig. 10(b), $K_n(q)=\tilde{u}_n/I$. By the first Kirchhoff's rule, the voltages at junctions in Fig. 10(b) satisfy

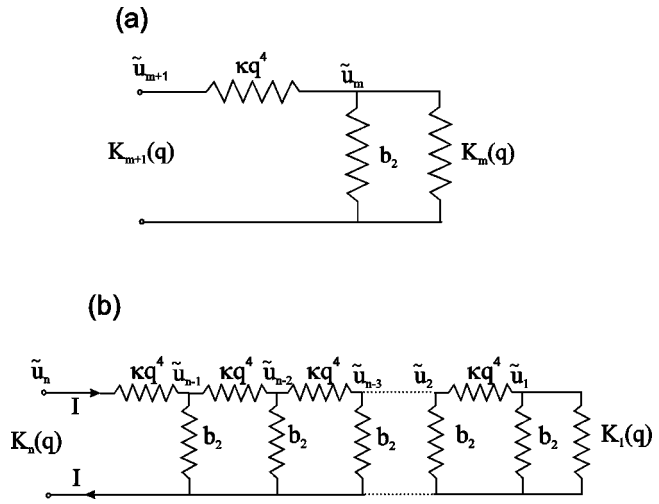

FIG. 10. (a) Simple circuit for the calculation of equivalent "resistance" $K_{m+1}(q)$. (b) Ladder circuit used for the calculation of the equivalent resistance $K_n(q) \equiv K_<(q)$.

$$\frac{\tilde{u}_{m+1}-\tilde{u}_m}{\kappa q^4}+\frac{\tilde{u}_{m-1}-\tilde{u}_m}{\kappa q^4}=\frac{\tilde{u}_m}{b_2}, \quad m=2,3,\ldots,n-1. \tag{A13}$$

Physically, the voltages in Eq. (A13) correspond to smectic phonon displacements $\tilde{u}_m(\mathbf{q})$ in Eq. (A9) [in fact, Eq. (A13) can be more directly obtained by varying Eq. (A9) over $\tilde{u}_m(\mathbf{q})$]. Equation (A13) can be solved by setting

$$\tilde{u}_m = A_1 R_1^m + A_2 R_2^m. \tag{A14}$$

From Eqs. (A13) and (A14), one finds the characteristic equation for R_1 and R_2 of the form

$$R-2+\frac{1}{R}=\frac{\kappa q^4}{b_2}. \tag{A15}$$

From Eq. (A15),

$$R_1(q)=\frac{1}{R_2(q)}=1+\frac{\kappa q^4}{2b_2}-\sqrt{\left(1+\frac{\kappa q^4}{2b_2}\right)^2-1}<1. \tag{A16}$$

The equivalent resistance $K_n(q)=\tilde{u}_n/I$ can be obtained by invoking two "boundary conditions" [obvious from Fig. 10(b)],

$$I=\frac{\tilde{u}_n-\tilde{u}_{n-1}}{\kappa q^4}=\frac{\tilde{u}_n}{K_n(q)} \tag{A17}$$

and

$$\tilde{u}_1=\frac{\dfrac{b_2 K_1(q)}{b_2+K_1(q)}}{\kappa q^4+\dfrac{b_2 K_1(q)}{b_2+K_1(q)}}\tilde{u}_2. \tag{A18}$$

From Eqs. (A14)–(A18), we obtain the final form of $K_n(q)=\tilde{u}_n/I$ as

$$K_n(q)=b_2\left(\frac{1}{R_1}-1\right)\frac{1+\dfrac{Z}{R_1}R_1^{2(n-1)}}{1-\dfrac{Z}{R_1^2}R_1^{2(n-1)}}. \tag{A19}$$

For $K_1(q)=K_{surf}^{(1)}(q)=\gamma q^2+\kappa q^4$, as in Sec. II, the quantity Z in Eq. (A19) has the form

$$Z(R_1)=R_1^2\frac{\bar{\gamma}\sqrt{R_1}-R_1}{\bar{\gamma}\sqrt{R_1}+1} \tag{A20}$$

with $\bar{\gamma}=\gamma/\sqrt{\kappa b_2}$. On the other hand, for the more general interface dispersion relation discussed in Ref. [29], of the form

$$K_1(q)=K_{surf}^{(1)}(q)=\kappa q^4+\frac{b_2^{(surf)}(\kappa' q^4+\gamma q^2)}{b_2^{(surf)}+\kappa' q^4+\gamma q^2}, \tag{A21}$$

Z in Eq. (A19) has the form

$$Z(R_1)=R_1^2\frac{\left[\dfrac{\kappa'}{\kappa}(1-R_1)+\bar{\gamma}\sqrt{R_1}\right]\left[1-(1-R_1)\dfrac{b_2}{b_2^{(surf)}}\right]-R_1}{\left[\dfrac{\kappa'}{\kappa}(1-R_1)+\bar{\gamma}\sqrt{R_1}\right]\left[1+\dfrac{1-R_1}{R_1}\dfrac{b_2}{b_2^{(surf)}}\right]+1}. \tag{A22}$$

Now we are in the position to consider the whole stack of manifolds. The $N-n$ manifolds above the $(n+1)$th manifold can be treated in a similar way as the manifolds below the nth manifold. This eventually yields the effective Hamiltonian for $\tilde{u}_n(\mathbf{q})$ and $\tilde{u}_{n+1}(\mathbf{q})$ of the form

$$\begin{aligned} H_{eff}(u_n,u_{n+1})=\int_q \frac{1}{2}[&K_<(q)|\tilde{u}_n(\mathbf{q})|^2 \\ &+b_2|\tilde{u}_{n+1}(\mathbf{q})-\tilde{u}_n(\mathbf{q})|^2 \\ &+K_>(q)|\tilde{u}_{n+1}(\mathbf{q})|^2], \end{aligned} \tag{A23}$$

with $K_<(q)=K_n(q)$, as in Eq. (A19), whereas

$$K_>(q)=b_2\left(\frac{1}{R_1}-1\right)\frac{1+\dfrac{Z}{R_1}R_1^{2(N-n-1)}}{1-\dfrac{Z}{R_1^2}R_1^{2(N-n-1)}}. \tag{A24}$$

Having the harmonic effective Hamiltonian in Eq. (A23), we finally obtain

$$\langle |u_{n+1}(\mathbf{x})-u_n(\mathbf{x})|^2\rangle_0 = k_B T \int_q \frac{1}{\dfrac{K_<(q)K_>(q)}{K_<(q)+K_>(q)}+b_2}$$

$$= \frac{k_B T}{b_2}\int \frac{d^d q}{(2\pi)^d}\frac{2\left(1-\dfrac{Z^2}{R^3}R^{2(N-2)}\right)+\dfrac{Z}{R^2}(R-1)(R^{2(n-1)}+R^{2(N-1-n)})}{\left(1+\dfrac{1}{R}\right)\left(1-\dfrac{Z^2}{R^2}R^{2(N-2)}\right)}. \tag{A25}$$

(For simplicity, here and now on, we write R instead of R_1.) For $d<4$, in the continuum limit $Q_{max}\sim 1/\Delta x\to\infty$, the integration over $q(0<q<\infty)$ in Eq. (A25) can be conveniently converted into the integration over R $(1>R>0)$ with the aid of relation between q and R in Eq. (A15), yielding

$$\langle [u_{n+1}(\mathbf{x})-u_n(\mathbf{x})]^2\rangle = \frac{S_d}{(2\pi)^d}\frac{k_B T}{2b_2}\left(\frac{b_2}{\kappa}\right)^{d/4} I_N(n,d,\bar{\gamma}) \tag{A26}$$

with S_d being the d-dimensional unit sphere area and $I_N(n,d,\bar{\gamma})$ as in Eq. (2.15). After the summation over n, we get the average for the whole stack

$$\frac{1}{N-1}\sum_{n=1}^{N-1}\langle |u_{n+1}(\mathbf{x})-u_n(\mathbf{x})|^2\rangle = \frac{S_d}{(2\pi)^d}\frac{k_B T}{2b_2}\left(\frac{b_2}{\kappa}\right)^{d/4} I_N(d,\bar{\gamma}) \tag{A27}$$

with $I_N(d,\bar{\gamma})$ as in Eq. (2.16). By combining Eqs. (A26) and (A27) with Eqs. (2.7) and (2.8), we eventually find our results in Eqs. (2.10)–(2.12), with $I_N(n,d,\bar{\gamma})$ and $I_N(d,\bar{\gamma})$ therein as in Eqs. (2.15)–(2.16). Therein, Z has the form as in Eq. (2.17), for the interface dispersion relation in Eq. (2.4). For a more general interface dispersion relation in Eq. (A21), Eqs. (2.15) and (2.16) are to be used with Z as in Eq. (A22).

For the two special values of $\bar{\gamma}=0$ or ∞, the average in Eq. (A26) can be calculated also by diagonalizing the harmonic Hamiltonian (A9) [for $\bar{\gamma}\neq 0,\infty$, the eigenvalue problem cannot be solved exactly]. This diagonalization yields the following interesting results:

$$I_N(n,d,\bar{\gamma}) = \frac{\pi}{\sin\left(\dfrac{d}{4}\pi\right)2^{1-d/4}}\Psi_N(n,d,\bar{\gamma}) \quad (\bar{\gamma}=0 \text{ or } \infty) \tag{A28}$$

with

$$\Psi_N(n,d,\bar{\gamma}=0) = \frac{1}{N}\sum_{m=1}^{N-1}\left[1-\cos\left(\frac{m\pi}{N}\right)\right]^{d/4} \times\left[1-\cos\left(\frac{2m\pi}{N}n\right)\right] \tag{A29}$$

and

$$\Psi_N(n,d,\bar{\gamma}=\infty) = \frac{1}{N-1}\sum_{m=1}^{N-2}\left[1-\cos\left(\frac{m\pi}{N-1}\right)\right]^{d/4} \times\left[1+\cos\left(\frac{2m\pi}{N-1}\left\{n-\frac{1}{2}\right\}\right)\right], \tag{A30}$$

Also, we find

$$I_N(d,\bar{\gamma}) = \frac{\pi}{\sin\left(\dfrac{d}{4}\pi\right)2^{1-d/4}}\Psi_N(d,\bar{\gamma}) \tag{A31}$$

with

$$\Psi_N(d,\bar{\gamma}=0) = \frac{1}{N-1}\sum_{m=1}^{N-1}\left[1-\cos\left(\frac{m\pi}{N}\right)\right]^{d/4} \tag{A32}$$

and

$$\Psi_N(d,\bar{\gamma}=\infty) = \frac{1}{N-1}\sum_{m=1}^{N-2}\left[1-\cos\left(\frac{m\pi}{N-1}\right)\right]^{d/4}. \tag{A33}$$

Using Eqs. (A28)–(A33), one can show the following interesting relations between the systems with zero and infinite surface tension:

$$I_{N+1}(d,\bar{\gamma}=\infty) = \frac{N-1}{N}I_N(d,\bar{\gamma}=0) \tag{A34}$$

and

$$I_{N+1}(n+\tfrac{1}{2},d,\bar{\gamma}=\infty) = 2I_{N+1}(d,\bar{\gamma}=\infty) - I_N(n,d,\bar{\gamma}=0). \tag{A35}$$

Using Eq. (A35), we find for semi-infinite smectics ($N\to\infty$),

$$\Delta(n+\tfrac{1}{2},d,\overline{\gamma}=\infty)=-\Delta(n,d,\overline{\gamma}=0), \tag{A36}$$

with $\Delta(n,d,\overline{\gamma})=I_\infty(n,d,\overline{\gamma})-I_\infty(d)$ as in Eq. (2.26). From Eqs. (A36) and (2.25), for inter-layer distances in semi-infinite systems, we find the relation

$$a_\infty\left(n+\tfrac{1}{2},\gamma=\infty\right)-a_\infty=-[a_\infty(n,\gamma=0)-a_\infty]$$

to be true for any d (to one-loop order), as exemplified before in Sec. II, for $d=2$ [see Eq. (2.28) and below]. For finite but large smectic stacks ($N\gg 1$), the expansion in Eq. (2.29) was useful on our discussion of Sec. II and III. By using Eq. (A34), the coefficients of this expansion can be related between the systems with infinite and zero tension. Thus we find

$$C_1(d,\overline{\gamma}=\infty)=C_1(d,\overline{\gamma}=0)-I_\infty(d) \tag{A37}$$

with $I_\infty(d)=B(1-d/4,d/2)$ as in the discussions of Sec. II. For $d=2$, $I_\infty(d=2)=B(1/2,1)=2$, and Eq. (A37) is in accord with the exact limits of C_1, which can be obtained by Eq. (2.32) yielding $C_1(d=2,\overline{\gamma}=0)=-\pi/2+2$ and $C_1(d=2,\overline{\gamma}=\infty)=-\pi/2$. For $d=1$, $I_\infty(d=1)=B(3/4,1/2)\cong 2.3963$, and Eq.(A37) is in accord with the numerical results for the limits of C_1, which can be obtained by Eq. (2.32) yielding $C_1(d=1,\overline{\gamma}=0)\cong 0.82$ and $C_1(d=1,\overline{\gamma}=\infty)\cong -1.56$, see Fig. 5.

For the physically interesting case of the smectic stack of membranes ($d=2$), the sums in Eqs. (A29), (A30), (A32), and (A33) can be done analytically. Indeed, by using the identity $\sqrt{1-\cos\theta}=\sqrt{2}\sin(\theta/2)$, one can see that these sums reduce to doable geometric (trigonometric) sums. In this way, we obtain the results in Eqs. (2.21)–(2.24). We stress that the results for $I_N(n)$ in Eqs. (2.21)–(2.24) are given for integer n (which is, of course, the physical case). For a non-integer n, $I_N(n)$ contains also some additional terms proportional to $\sin(2\pi n)$, and $1-\cos(2\pi n)$, vanishing for integer n. We are not going to display these terms here, as they are not of physical significance. Still we note their existence for a noninteger n, for the readers trying to check our Eq. (A35) (that requires replacement $n\to n+1/2$), by naively using the expressions in Eqs. (2.23) and (2.24), which apply only for integer n.

As noted in Sec. II, the above formulas are applicable for $d<4$, when the momentum integral in Eq. (A26) has finite continuum limit, i.e., one can set the upper momentum cutoff therein, $Q_{max}=2\pi/\Delta x\to\infty$. In fact, to all orders of perturbation theory, the continuum limit $\Delta x\to 0$ is finite for $d<4$, because the dispersion relations for all manifolds (including also the interfacial manifolds) grow as q^4 for large q. Consequently, in our theory, the cutoff Q_{max} plays no substantial role for the VPP phenomena. In fact, by repeating our analytic calculations with a finite $Q_{max}=2\pi/\Delta x$, the relative error ($\mathcal{E}$) done by assuming $\Delta x=0$ can be shown to be small for $d<4$, of the order

$$\mathcal{E}=\left(\frac{\Delta x}{L_b}\right)^{4-d}. \tag{A38}$$

Here L_b is the smectic healing length, $L_b=(\kappa/b_2)^{1/4}$ (see Ref. [12]). For example, for sterically stabilized stacks (as well as for strongly entropic bound stacks, see Fig. 6 and Sec. III), L_b coincides with the distance between ''collisions'' of a manifold with its neighbors, and thus $(a-a_{min})^2=l^2\approx(k_BT/\kappa)(L_b)^{4-d}$. Thus, by using Eq. (A38),

$$\mathcal{E}=\frac{k_BT}{\kappa}\frac{(\Delta x)^{4-d}}{l^2}. \tag{A39}$$

Therefore, for example, for 3D stacks of membranes ($d=2$), $\mathcal{E}$ in Eq. (A39) is small because, typically, $k_BT/\kappa\sim 1/10$ (see Sec. II), and the intermembrane separation (water gap) is in the range $l=1-100$ nm, whereas $\Delta x\approx 1$ nm (the lipid molecule size). We stress that, by Eq. (A39) with $d=2$, *already* at the lower limit of the water gap range ($l\approx 1$ nm), the molecular scale (cutoff) effect is small for realistic bilayer membranes in lamellar phases, with $\kappa>10k_BT$. Thus, in particular, the theory of Ref. [14] fails to provide the correct account of cutoff effects *even* for small intermembrane separations in realistic systems.

APPENDIX B:

In this appendix we consider smectic stacks with N manifolds in the limit of infinite surface tension of the interfacial manifolds (the first and the last manifolds of the stack). In this limit, the interfacial manifolds behave as infinitely rigid (and thus flat) but still mobile manifolds ''pistons'' whose equilibrium distance $L=\langle h_N-h_1\rangle$ adjusts according to the applied value of the osmotic pressure P. Since the manifolds are flat, $h_N(\mathbf{x})-h_1(\mathbf{x})$ does not depend on $\mathbf{x}$, and this problem becomes exactly equivalent (in the $\gamma\to\infty$ limit) to the problem of $N_k=N-2$ manifolds confined between two hard walls of the distance L.

This feature can be used to extract the constants $\beta_N(d,\gamma)$, in the limit $\gamma\to\infty$, from some of the previous knowledge on the stacks of $N_k=N-2$ manifolds confined between two hard walls at the distance $L=\langle h_N-h_1\rangle=(N-1)a_N$, in the notation of the present paper. For simplicity, let us set $a_{min}=0$ and $\kappa=k_BT=1$, as this is possible to achieve by a suitable rescaling (similar to that used in Sec. III).

Let us first consider the stack with $N=3$ semiflexible polymers ($d=1$) fluctuating in a plane. In the limit $\gamma\to\infty$, this problem reduces to the problem of a single semiflexible polymer fluctuating between two hard walls at distance L. By using the exact result of Burkhardt [21], for this problem we have the osmotic pressure

$$P=\frac{2}{3}\frac{A_B}{L^{5/3}} \tag{B1}$$

with $A_B\cong 1.1036$, as found by Burkhardt from an analytic transfer matrix calculation. Thus the distance between two hard walls is

$$L=\left(\frac{2}{3}A_B\right)^{3/5}\frac{1}{P^{3/5}}. \tag{B2}$$

TABLE I. The first column gives the universal constants $\beta_N(d=2,\gamma=\infty)$ obtained by using Eq. (B7), as explained in Appendix B. The second column gives the one-loop fit to data in the first column, with $\beta_\infty=0.595$ and $A'_{d=2}=0.190$, see Appendix B, Eq. (B8).

N	$\beta_N(d=2,\gamma=\infty)$	$\beta_\infty(d=2)+A'_{d=2}[I_N(d=2,\gamma=\infty)-I_\infty(d=2)]$
3	0.426	0.426
4	0.487	0.487
5	0.516	0.515
6	0.532	0.532
7	0.543	0.543
8	0.550	0.551
9	0.556	0.556
10	0.560	0.561
11	0.564	0.564
12	0.567	0.567
13	0.569	0.569
14	0.571	0.572
15	0.572	0.573
16	0.574	0.575
17	0.575	0.576

By using here $L=\langle h_N-h_1\rangle=(N-1)a_N$, with $N=3$, we have

$$a_{N=3}=\frac{L}{2}=\frac{1}{2}\left(\frac{2}{3}A_B\right)^{3/5}\frac{1}{P^{3/5}}. \tag{B3}$$

By comparing Eq. (B3) with Eq. (3.16) (with $a_{min}=0$ and $\kappa=k_BT=P=1$), we obtain the exact value of $\beta_N(d,\gamma)$ for $N=3$, $d=1$, and $\gamma=\infty$,

$$\beta_{N=3}(d=1,\gamma=\infty)=\frac{1}{2}\left(\frac{2}{3}A_B\right)^{3/5}. \tag{B4}$$

This equation, with $A_B=1.1036$, yields $\beta_{N=3}(d=1,\gamma=\infty)\cong 0.416$, as stated in Eq. (3.24).

We used the same reasoning to extract $\beta_N(d=2,\gamma=\infty)$, by using the results of Bachmann *et al.* [22] for the stack of $N_k=N-2$ membranes fluctuating between two hard walls at distance L (corresponding, in our case, to the interfacial membranes with $\gamma=\infty$). Reference [22] gives the results for the osmotic pressure in the form (again we set $\kappa=k_BT=1$ and $a_{min}=0$)

$$P=\frac{2N_k}{N_k+1}\alpha^{(hw)}_{N_k}\frac{1}{[L/(N_k+1)]^3}. \tag{B5}$$

Here, $\alpha^{(hw)}_{N_k}$ are the "hard-wall" universal constants tabulated in Ref. [22]. See Table III therein. Pay attention that here we denote the number of membranes between hard walls as N_k, to distinguish it from the total number of membranes here $=N=N_k+2$, which includes also the hard walls corresponding here to infinitely rigid interfacial membranes at distance $L=\langle h_N-h_1\rangle$. By using Eq. (B5), with $N_k=N-2$,

$$a_N=\frac{\langle h_N-h_1\rangle}{N-1}=\frac{L}{N-1}=\left[\frac{2(N-2)}{N-1}\alpha^{(hw)}_{N-2}\right]^{1/3}\frac{1}{P^{1/3}}. \tag{B6}$$

By comparing Eq. (B6) with Eq. (3.16) (with $\kappa=k_BT=P=1$ and $a_{min}=0$), we obtain the values of $\beta_N(d,\gamma)$ for $d=2$ and $\gamma=\infty$ in the form

$$\beta_N(d=2,\gamma=\infty)=\left[\frac{2(N-2)}{N-1}\alpha^{(hw)}_{N-2}\right]^{1/3}. \tag{B7}$$

Here, the values of $\alpha^{(hw)}_{N_k}$ are given in the Table III of Ref. [22], for $N-2=1$ through 15. By using that table, and our Eq. (B7), we obtain our Table I, with $\beta_N(d=2,\gamma=\infty)$, for $N=3$ through 17. The table documents the fact that these constants are well approximated by the one-loop formula

$$\begin{aligned}\beta_N(d=2,\gamma=\infty)&=\beta_\infty(d=2)+A'_{d=2}[I_N(d=2,\gamma=\infty)-I_\infty(d=2)]\\&=\beta_\infty(d=2)-A'_{d=2}\frac{\frac{1}{2}\pi}{N}+\cdots,\end{aligned} \tag{B8}$$

with $\beta_\infty(d=2)\cong 0.595$ and $A'_{d=2}\cong 0.190$, as employed in the discussions of Sec. III. We recall that here $I_\infty(d=2)=2$ and $I_N(d=2,\gamma=\infty)$ is exactly given by Eq. (2.22).

[1] J. Toner and D.R. Nelson, Phys. Rev. B **23**, 316 (1981).

[2] C.R. Safinya, D. Roux, G.S. Smith, S.K. Sinha, P. Dimon, N.A. Clark, and A.M. Bellocq, Phys. Rev. Lett. **57**, 2718 (1986); see also D. Roux and C.R. Safinya, J. Phys. (Paris) **49**, 307 (1988).

[3] L. Golubović and Z.-G. Wang, Phys. Rev. Lett. **69**, 2535 (1992); Phys. Rev. E **49**, 2567 (1994).

[4] J.O. Rädler, I. Koltover, T. Saldit, and C.R. Safinya, Science **275**, 810 (1997).

[5] T. Salditt, I. Koltover, J.O. Rädler, and C.R. Safinya, Phys. Rev. Lett. **79**, 2582 (1997); Phys. Rev. E **58**, 889 (1998).

[6] F. Artzner, R. Zantl, G. Rapp, and J. Rädler, Phys. Rev. Lett. **81**, 5015 (1998); R. Zantl, F. Artzner, G. Rapp, and J.O. Rädler, Europhys. Lett. **45**, 90 (1990).

[7] L. Golubović and M. Golubović, Phys. Rev. Lett. **80**, 4341 (1998); **81**, 5704(E) (1998); C.S. O'Hern and T.C. Lubensky, *ibid.* **80**, 4345 (1998).

[8] L. Golubović, T.C. Lubensky, and C.S. O'Hern, Phys. Rev. E **62**, 1069 (2000).

[9] L. Golubović, Phys. Rev. E **64**, 061901 (2001).

[10] W. Helfrich, Z. Naturforsch. A **33**, 305 (1978); W. Helfrich and R.M. Servus, Nuovo Cimento D **3**, 137 (1984).

[11] L. Gao and L. Golubović, Phys. Rev. E **66**, 051918 (2002); See also, Ref. [9].

[12] L. Gao and L. Golubović, Phys. Rev. E **67**, 021708 (2003).
[13] P. G. de Gennes and J. Prost, *Physics of Liquid Crystals* (Oxford University Press, Oxford, 1993), see Chap. 7; P.G. de Gennes, Europhys. Lett. **13**, 709 (1990).
[14] R. Podgornik and V.A. Parsegian, Biophys. J. **72**, 942 (1997); V.A. Parsegian and R. Podgornik, Colloids Surf., A **130**, 345 (1997).
[15] See, for example, M. Manciu and E. Ruckenstein, Langmuir **18**, 4179 (2002); R. Podgornik and V.A. Parsegian, *ibid.* **8**, 557 (1992).
[16] H.I. Petrache, N. Gouliaev, S. Tristram-Nagle, R. Zhang, R.M. Suter, and J.F. Nagle, Phys. Rev. E **57**, 7014 (1998).
[17] J. Katsaras, Biophys. J. **73**, 2924 (1997); J. Katsaras, *ibid.* **75**, 2157 (1998); These systematic experimental studies report no visible VPP phenomena in bound stacks of DMPC bilayers, in contrast to earlier experimental observations [see, e.g., G.S. Smith, C.R. Safinya, D. Roux, and N.A. Clark, Mol. Cryst. Liq. Cryst. **144**, 235 (1987)].
[18] J.F. Nagle and J. Katsaras, Phys. Rev. E **59**, 7018 (1999).
[19] J.F. Nagle and S. Tristram-Nagle, Biochim. Biophys. Acta **1469**, 159 (2000).
[20] R.R. Netz, Phys. Rev. E **51**, 2286 (1995); R.R. Netz and R. Lipowsky, Europhys. Lett. **29**, 345 (1995). They calculate $\beta_N(\bar{\gamma},d=2)$ for $\bar{\gamma}=0$ and $N=2$ with the result $\beta_2(\bar{\gamma}=0,d=2)=0.614$. Our Eq. (3.28) yields $\beta_2(\bar{\gamma}=0,d=2)=0.637$.
[21] T.W. Burkhardt, J. Phys. A **30**, L167 (1997).
[22] M. Bachmann, H. Kleinert, and A. Pelster, Phys. Rev. E **63**, 051709 (2001).
[23] G. Gompper and D.M. Kroll, Europhys. Lett. **9**, 59 (1989).
[24] L.V. Mikheev, Sov. Phys. JETP **69**, 358 (1989).
[25] A. Ajdari, B. Duplantier, D. Hone, L. Peliti, and J. Prost, J. Phys. II **2**, 487 (1992).
[26] R. Holyst, D.J. Tweet, and L.B. Sorensen, Phys. Rev. Lett. **65**, 2153 (1990); R. Holyst, Phys. Rev. A **44**, 3692 (1991); see also, V.P. Romanov and S.V. Ul'yanov, Phys. Rev. E **63**, 031706 (2001); Experimental studies of smectic stacks have been extensively conducted by de Jeu and co-workers. See, J.D. Shindler *et al.*, Phys. Rev. Lett. **74**, 722 (1995); E.A.L. Mol *et al.*, *ibid.* **79**, 3439 (1997); A. Fera *et al.*, *ibid.* **85**, 2316 (2000). We stress that, within the harmonic stack model, average smectic interlayer distances are uniform in finite stack. Their nonuniformity may emerge due to the anharmonic effects discussed in our study here. In this respect, our anharmonic thermomechanical finite-size VPP effects are different from the nonuniformity of, for example, smectic displacement fluctuations, $\langle (u_n)^2 \rangle$, which are nonuniform (n dependent) already in the harmonic stack model. It is thus misleading to associate VPP effects with the nonuniformity of displacement fluctuations $\langle (u_n)^2 \rangle$, as done in qualitative discussions made in Ref. [14]. In fact, VPP is an anharmonic effect, and the nonuniformity of interlayer distances is directly related to the nonuniformity of *strain fluctuations* $\langle (u_{n+1}-u_n)^2 \rangle_0$, as manifested by our anharmonic theory [see our Eq. (2.7)].
[27] N. Lei, C.R. Safinya, and R. Bruinsma, J. Phys. II **5**, 1155 (1995).
[28] M. Vogel, C. Münster, W. Fenzl, and T. Salditt, Phys. Rev. Lett. **84**, 390 (2000).
[29] L. Gao and L. Golubović (unpublished).